Actuation Techniques
For
Frequency Modulated MEMS Gyroscopes

by

Michael Xie

A thesis
presented to the University of Waterloo
in fulfillment of the
thesis requirement for the degree of
Master of Applied Science
in
Mechanical Engineering

Waterloo, Ontario, Canada, 2015

AUTHOR'S DECLARATION

I hereby declare that I am the sole author of this thesis. This is a true copy of the thesis, including any required final revisions, as accepted by my examiners.

I understand that my thesis may be made electronically available to the public.

Abstract

This thesis focuses on the design and implementation of an analog actuation circuit for a novel frequency-modulated MEMS gyroscope. The gyroscope detects angular rotations as the difference between the natural frequencies of two closely spaced drive and sense modes rather than the magnitude of displacement in the sense direction. Furthermore, the actuation system features a resonant drive (RLC) circuit that amplifies the gyroscope actuation signal. The input to the circuit is an amplitude-modulated (AM) signal composed of a carrier signal modulated with a base signal that excites the gyroscope drive mode. The carrier frequency corresponds to the electrical resonance frequency of the drive circuit. This research develops techniques for the stabilization of the circuit output through close loop feedback.

First, we attempt to increase the signal-to-noise ratio of the modulating signal by implementing feedback and feedforward control loops (AGC). The feedback controller closes the loop on the entire conditioning circuit for the modulating signal while the feedforward controller acts on the input signal to the conditioning circuit. The feedforward and the feedback controllers derive an error signal representing the signal noise by comparing the input and output signal, respectively, with a reference signal. However, we find that the breadboard circuit implementations of our control strategies performed similar to a baseline uncontrolled function generator due to the additional noise input from the breadboard and the additional components used to implement the controller, such as the amplifiers.

Next, we develop a single-harmonic amplitude-stabilized actuation scheme for the gyroscope to minimize multi-frequency excitations and reduce amplitude fluctuations to improve the gyroscope precision. A low pass filter is applied to the AM signal to obtain a single sideband full carrier (SSB-FC) signal. Since the capacitance of RLC circuit changes due to the vibration of the gyroscope, this variation in capacitance causes a shift in the frequency response of the RLC circuit, resulting in variation in the circuit gain. Three feedback control topologies are implemented to stabilize the signal by first detecting the change in signal level, and then amplifying or attenuating the signal level in order to maintain a constant gyroscope actuation level. The control strategy with the best performance involves feeding back the RMS of the output signal to control the amplitude of the carrier signal and feeding back the average of the output signal's envelope to control the bias level of the modulating signal. Using control this strategy, the peak magnitude at the carrier frequency dropped approximately 2% as the capacitance is varied from 15 pF to 16 pF, awhile the other two control strategies changed 9% and 6%.

Acknowledgements

I would like to show my sincere gratitude to my supervisors, Prof. Mustafa Yavuz and Prof. Eihab Abdel-Rahman, who has given me great guidance and support, making this research possible. I would also like to thank Prof. Baris Fidan and Prof. Armaghan Salehian for being the examiners for my thesis.

I am also truly grateful of the assistance from all of my colleagues: Sangtak Park, Mahmoud Khater, Muhammed Altaher, Hamidreza Nafissi, Mohammed Bendame, David Effa, Turker Dagdelen, Resul Saritas, Bassam Tunkar, Majed Alghamdi, Karim Elrayes, Raed Alharbi, Savas Ozdemir, and Rasit Atelge.

I also deeply appreciate the help and support which my family and friends have given me.

Dedication

I dedicate this thesis to my parents for their support, guidance and love, which mold me into who I am today.

Table of Contents

List of Figures

List of Tables

Chapter 1
Introduction

1.1 MEMS gyroscopes

Micro-electromechanical systems (MEMS) combine micromachining with silicon-based microelectronics, which are fabricated using integrated circuit (IC) techniques. Micromachining can be described as an extended IC fabrication technique involving advanced process techniques such as photo-fabrication, deep etching, and anodic bonding [1]. MEMS technology is essential to recent technological advances, especially in applications where portability is a key concern. MEMS components have physical size within the range of microns to millimeters and are used in many applications such as sensors, actuators and control systems. Their primary advantages are their small size, light weight, low cost and power efficiency.

An example is the MEMS gyroscope, which is fabricated by surface micromachining and mounted on a chip with the controlling IC. These inertial rate sensors can be used to measure the angle or angular velocity in a variety of applications. In consumer electronics, such as cell phones, tablets and laptops, many programs and applications require sensing the angular velocity of the device for interacting with the user; for example, games, real-time physics simulation and even basic screen rotation. For automobiles and aircrafts, gyroscope alongside with accelerometer and GPS are a part of the inertial navigation systems (INS), which is used to measure and calculate the navigation route without the need of any external references. The angular position can be measured by integrating the angular velocity with respect to time. However, integration drift is a critical concern for many MEMS gyroscopes since minor errors in angular velocity accumulates over time while calculating the angular position.

MEMS gyroscopes are also essential elements for stabilization, acting as the sensor in a feedback control system. Examples of gyroscopic stabilization are rollover prevention systems in automobiles and image stabilization for cameras.

1.1.1 Coriolis effect

The fundamental physical principle behind a vibratory gyroscope is the Coriolis effect [2]. As an object with mass m, moves in a straight line away from the center of a rotating plate (or any rotating reference frame), there is a deflection of the particle in the perpendicular direction.

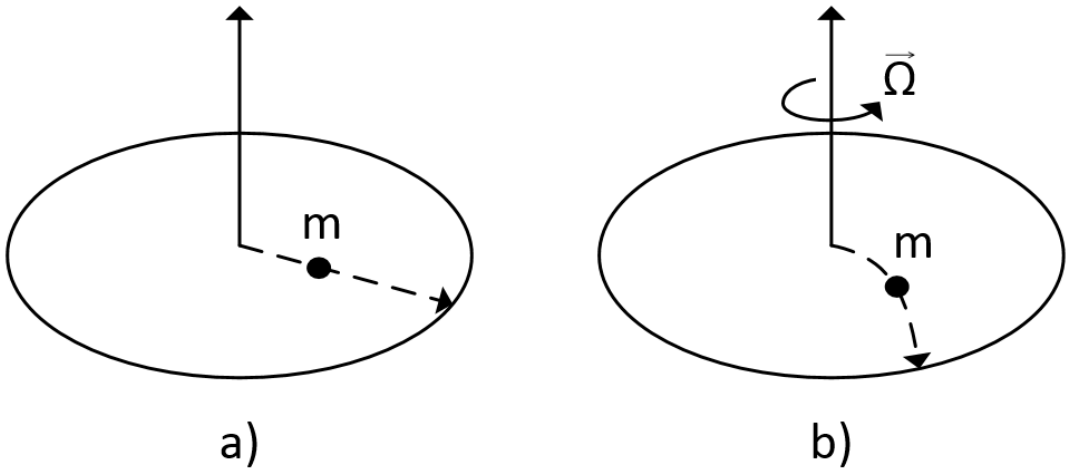

Figure 1.1. a) Object moving in a line away from the center of a plate. b) Movement of the particle is deflected due to rotation of plate (Coriolis effect).

The Coriolis acceleration can be described by:

$$\overrightarrow{a_c} = 2\overrightarrow{\Omega} \times \vec{v} \tag{1.1}$$

where $\overrightarrow{a_c}$ is the Coriolis acceleration of the object as its reference frame rotates, $\overrightarrow{\Omega}$ is the angular velocity vector of the frame as it rotates about its center axis, and $\vec{v}$ is the velocity of the object with respect to the rotating reference frame in a straight line away from the center. The Coriolis acceleration, $\overrightarrow{a_c}$, is perpendicular to $\vec{v}$. The Coriolis force $\overrightarrow{F_c}$, is,

$$\overrightarrow{F_c} = 2m(\overrightarrow{\Omega} \times \vec{v}) \quad (1.2)$$

where m is the mass of the object.

1.2 Types of MEMS Gyroscopes

There are two broad classification of micromachined gyroscopes: angle gyroscopes or rate gyroscopes [3]. An angle gyroscope directly measures the angular position (orientation). This type of gyroscopes requires free oscillation of a mass, which can be achieved by implementing energy sustaining feedback control to eliminate the effects of damping. Rate gyroscopes measure the angular rotation rate, which can be integrated over time to obtain the orientation. However, most currently reported micromachined vibratory gyroscopes (MVG) are rate gyroscopes [3] and they are of concern in this thesis.

1.3 Vibratory MEMS Gyroscope

MEMS vibratory rate gyroscopes use the Coriolis effect to the measure angular velocity. The gyroscope can be represented as a mass which initially vibrates in a drive direction actuated by an electrode, Figure 1.2. As the mass rotates about a fixed reference frame ($\boldsymbol{\xi}$-$\boldsymbol{\eta}$-$\boldsymbol{\zeta}$), the Coriolis force causes a displacement of the mass orthogonal to the drive direction. The value of this displacement can be sensed with another electrode and is directly related to the angular rate applied, as shown in Equation 1.2.

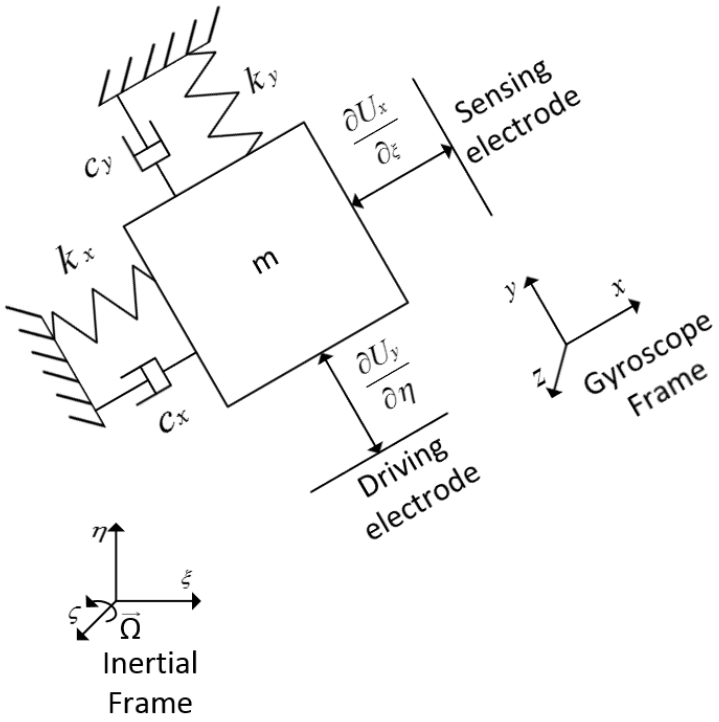

Figure 1.2. Model of a typical vibratory MEMS gyroscope rotating about an inertial frame.

When viewed from the inertial frame, the simplified equations of motion of a generalized vibratory gyroscope are [16]:

$$m\ddot{x} + c_x\dot{x} + k_x x = F_{es} + 2m\Omega\dot{y} \tag{1.3}$$

$$m\ddot{y} + c_y\dot{y} + k_y y = -2m\Omega\dot{x} \tag{1.4}$$

where m represents the effective mass, c represents the damping coefficient and k represents the spring stiffness. F_{es} represents the external electrostatic force applied by the drive electrode and Ω is the angular velocity.

In MEMS devices, one common method of sensing displacement is using capacitive sensing. The Coriolis effect couples the sense mode and the drive mode of the gyroscope mass. In addition,

conventional vibratory rate gyroscopes are designed to operate at or around their natural frequency such that they would have a higher sensitivity. Theoretically, if the reference frame is not rotating, there will be no displacement in the sense direction, but this is not the case for a real gyroscope due to different sources of errors.

1.4 Gyroscope Performance Parameters

There are several parameters to determine and evaluate the functionality of a gyroscope. The zero rate output or null output (^{o}/s) is defined as the output of gyroscope when no angular velocity is applied [5]. This is a measure of the bias drift or the bias stability of the gyroscope. The range of a gyroscope is the maximum angular velocity that it can measure. The sensitivity of a gyroscope (mV/ ^{o}/s) describes the resolution of gyroscope in terms of the relationship between the output voltage of gyroscope and its angular velocity. In essence, there is a tradeoff between the range and sensitivity of a gyroscope.

Almost all the gyroscopes are have noise from a variety of sources such as temperature, micromachining inaccuracies, sensitivity to acceleration [5]. Temperature can greatly affect the gyroscope's bias drift. These errors must be minimized using compensation such as integrated temperature sensors, external accelerometer and vibration rejection technology. The temperature can be tested by plotting the gyroscope's null output (^{o}/s) over a range of temperatures. In terms of acceleration sensitivity, g sensitivity (^{o}/s/g), and g^2 sensitivity (^{o}/s/g), are parameters which respectively define the sensitivity to linear acceleration and vibration rectification [5]. The g sensitivity is more significant for most devices since the field gravity of earth is 1g. Most of the high performance gyroscopes have g sensitivity of around 0.1 ^{o}/s/g.

1.4.1 Types of Vibratory MEMS Gyroscopes

Among different types of micro-scaled gyroscopes, the suspended vibratory are most favorable due to their manufacturability. They use a vibrating mechanical element to sense rotation. These devices does not require any bearings for its rotating parts; therefore making them suitable for micro-scaled

dimensions and batch micromachining techniques. Vibratory gyroscopes include tuning forks, vibrating beams, and vibrating shells [3].

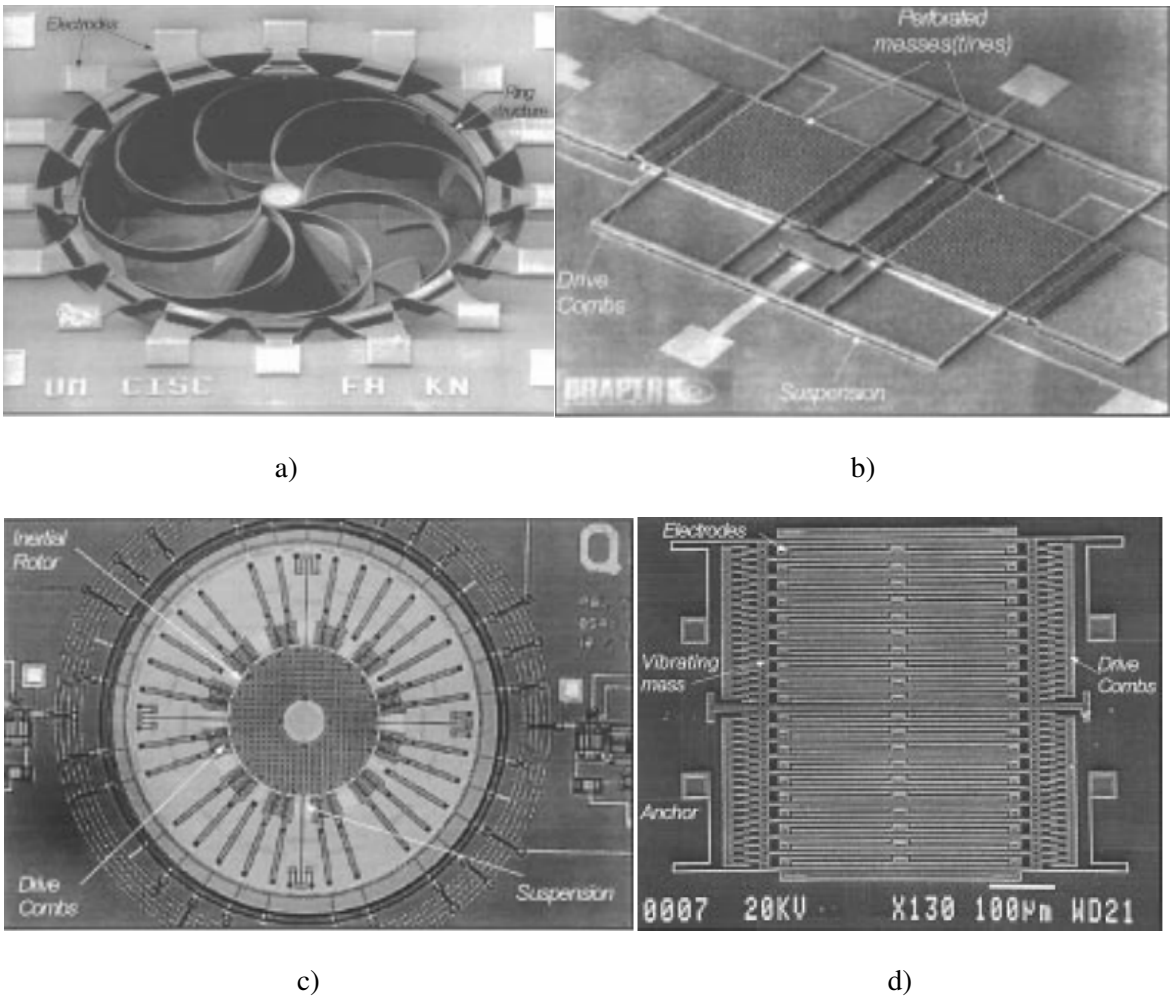

Figure 1.3. SEM pictures of different MEMS vibratory gyroscopes: a) vibrating ring [4] b) tuning fork [5] c) dual-axis [6] d) comb drive [7].

A tuning fork gyroscope is similar to a rotating system with two masses, giving a differential output and making the system insensitive to undesired linear vibration and acceleration acting on the gyroscope.

1.5 Frequency Modulated MEMS gyroscopes

Effa et al. [8] modeled a novel frequency modulated (FM) vibratory MEMS gyroscope and presented its fabrication process. The suspended MEMS cantilever beam supports a proof mass at its free end which is electrostatically coupled to one bottom and two side fixed electrodes, Figure 1.4. The bottom electrode excites vibrations along the drive mode in the x-direction and the side electrodes detect motions along the sense mode in y-direction. When the gyroscope base is rotated about the z-axis, Coriolis effect will be introduced, coupling the proof mass displacements in the drive and sense directions. Instead of measuring the amplitude of displacement in the sense direction, the FM gyroscope detects the difference between the frequencies of the closely spaced drive and sense modes, which is then used to measure the angular velocity.

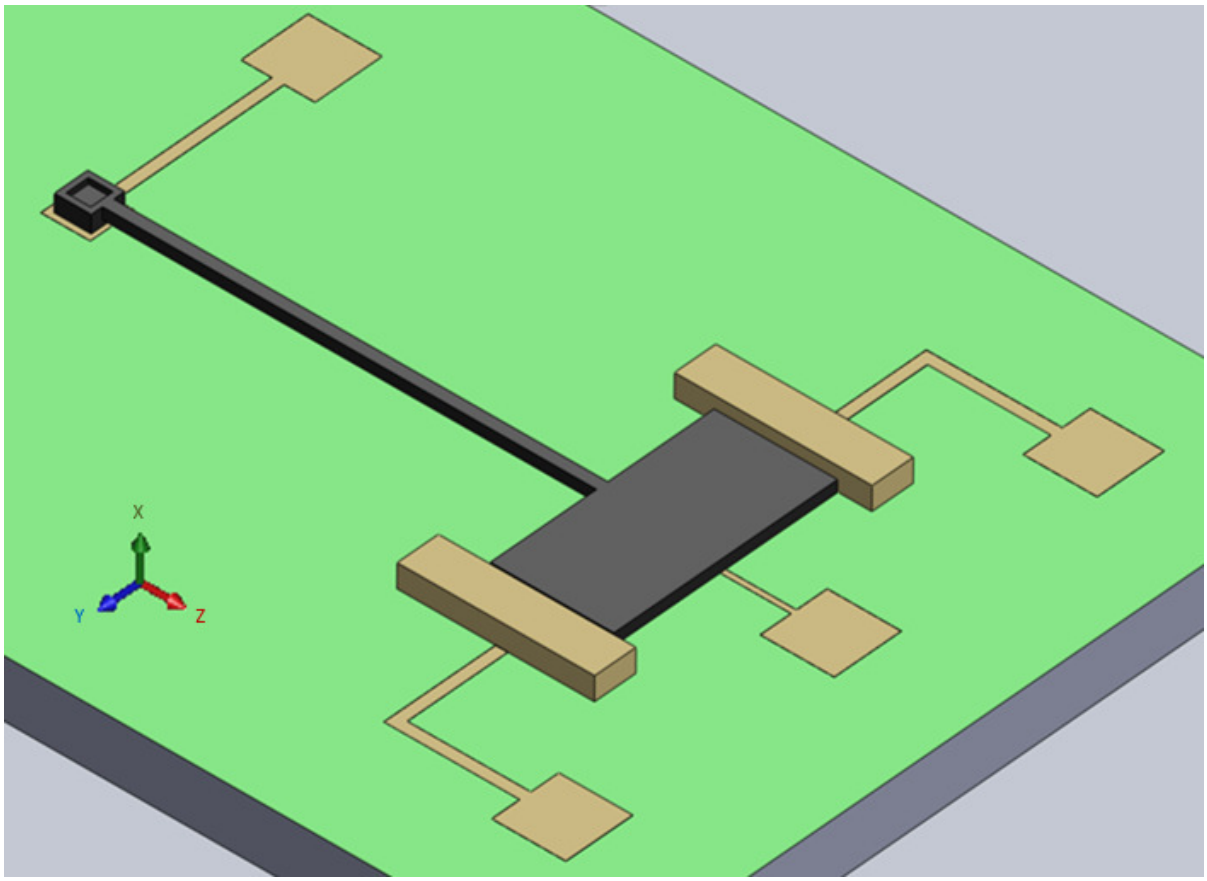

Figure 1.4. Model of MEMS gyroscope with drive mode along the x-direction and sense mode along the y-direction.

The functionality of the gyroscope depends on generating large motions in the drive mode at its natural frequency. This is advantageous to the system in terms of higher sensitivity, better linearity and lower power consumption.

1.6 Resonant Sensing

The proposed FM gyroscope uses a resonant sensing technique [8]. Resonance is the response of the gyroscope when it is excited at its natural frequency, at which the system will have a maximum conservation of its input energy. In a mechanical system such as a gyroscope, resonance can be observed as a dramatic increase in the amplitude of vibration; in an electrical system, resonance has a similar effect but in terms of the signal amplitude.

In resonant sensing, the natural frequency of the gyroscope will be shifted if its physical parameter varies, such a displacement in the sensing direction caused by Coriolis effect. This difference in frequency, compared to the drive frequency allows us to detect the motion of the gyroscope and in turn the angular velocity.

1.7 Resonant Drive

Not only can the resonance principle be beneficial for sensing, it can also be used for the electrostatic actuation [10-13] of the gyroscope. An RLC circuit is composed of a resistor, inductor and a capacitor and allows the electrical input energy to be conserved as well. The RLC circuit acts as a harmonic resonator, amplifying the current to the maximum if connected in parallel and the voltage if connected in series. For this thesis, maximizing the input voltage for the electrostatic actuator is of interest.

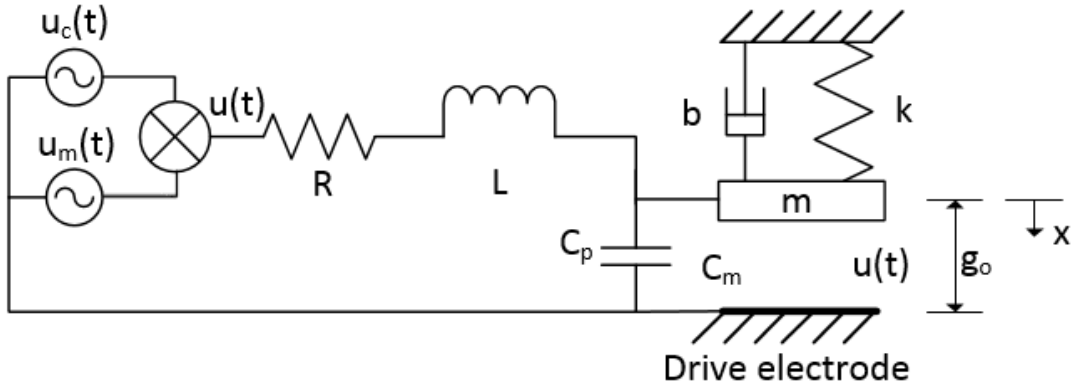

Figure 1.5. Diagram of MEMS gyroscope proof mass, drive electrode, and resonant drive circuit with AM input signal.

In order to both actuate the RLC circuit and oscillate the mechanical gyroscope at their natural frequencies, we use an amplitude-modulated (AM) actuation signal. The AM signal is the result of multiplying two signals: a carrier signal having the same frequency as the resonant frequency of the RLC circuit and a modulating signal having the same frequency as the natural frequency of the gyroscope. Using this signal, the RLC circuit will be able to amplify the input voltage awhile transferring the information regarding the natural frequency of the gyroscope to the mechanical system. Both the resonant drive circuit and the AM actuation signal will be discussed in detail in Chapter 3.

1.8 Objective

An analog circuit for the resonant drive of the FM gyroscope is to be designed and implemented. The circuit should provide an amplitude-modulated (AM) signal as the input into an RLC resonant drive circuit, which drives the gyroscope. In addition, the effects of different types of AM signals on the electrostatic force applied to the gyroscope is studied.

The actuation of MEMS gyroscopes require a stable input signal since any variation in the amplitude of the input signal would result in error in detection. However, the capacitance of RLC circuit will change due to the vibration of the gyroscope. This variation in capacitance will shift the frequency

response of the RLC circuit such that the oscillation will no longer be at the peak of the resonance, resulting in lower signal amplitude. A feedback control scheme must be designed and implemented to stabilize the signal by first detecting the change in signal level, and then amplify or attenuate the signal level such that the actuation signal driving the gyroscope remains constant.

Since the input signal is an amplitude modulated signal, the analog control scheme must be modified in comparison to conventional gain control methods. In addition, the effect of the control scheme on the noise floor of the signal is studied in attempt to reduce the noise floor of the actuation signal. In theory, a control system containing feedback should have an impact on lowering the noise floor since an error signal is feedback to the input signal. This error signal would contain information regarding the noise and as it is used to control the amplitude, it should counteract with the actual noise. Automatic gain control (AGC) circuits are conventionally used for stabilizing the amplitude of a signal under varying conditions; however, its effect on the actual noise floor of a signal is to be investigated.

1.9 Thesis Outline

Chapter 2 will cover the state of art regarding MEMS gyroscope actuation control, which can be broadly categorized as digital or analog control. Chapter 3 presents the resonant drive circuit with its AM actuation signal in detail. In addition, different types of AM and their effects on the electrostatic force which actuates the gyroscope are studied. Chapter 4 will describe feedfoward and feedback control of the actuation signal using AGC. Chapter 5 presents the circuit implementation both excluding and including the resonant drive circuit within the control loop. Results including noise floor comparison and amplitude stabilization are also presented and discussed. Chapter 6 concludes the thesis and looks at future works.

Chapter 2
Literature Review

2.1 Overall Gyroscope Control

For an operational gyroscope, there are several factors which require control. Firstly, the gyroscope should be kept oscillating at its natural frequency to initiate the oscillation to a suitable energy level and maintain the reached energy level [14]. Conventionally this is done by implementing a transresistance amplifier (TRA) in a positive feedback configuration and the oscillation amplitude is kept constant with an automatic gain control (AGC) loop.

In addition, quadrature deviation from the reference straight line of oscillation must be compensated. This is due to non-idealities in the gyroscope, such as fabrication irregularities, misalignment of the drive force and anisoeleasticity, which can cause ellipticity of the gyroscope trajectory [14]. This ellipticity (quadrature) can be used as a measurement of deviation from straight line oscillation and used for defining a quadrature compensating controller.

Furthermore, it must sense displacements and velocities in two perpendicular directions. This is traditionally performed by lateral and differential comb fingers or parallel plate capacitors. However, capacitive sensing requires the measurement of extremely small motions due to weak Coriolis force coupling between drive and sense modes. Methods have been developed to stabilize the electric actuation signal of MEMS gyroscopes in order to provide optimal sensitivity. These efforts can be classified into analog and digital drive mode control.

2.2 Gyroscope Drive Mode Control

2.2.1 Automatic Gain Control (AGC) and Phase Lock Loop (PLL)

Most of the conventional methods of actuation signal stabilization involve stabilizing of the signal amplitude using an automatic gain control (AGC) circuit while controlling the frequency with a phase-lock loop (PLL). Both of these control strategies involves comparing the input signal with a

reference signal. The result of the comparison is an error signal which is then used to control the input signal. The capacitive signal can be measured using a charge-sensitive amplifier (CSA) or transresistance amplifier (TRA), which amplifies the output current to a detectable voltage. The signal from the CSA can be used as the reference signal for the PLL, which is then connected to the AGC loop [17].

2.2.2 Adaptive Control

Several other control system approaches are used for the stabilization of MEMS gyroscope signal including using an extended state observer (ESO) in combination with active disturbance rejection control (ADRC) [18]. The dynamics of the gyroscope and disturbances are estimated using the ESO and the ADRC compensates for these errors in order to drive the gyroscope output to resonance.

2.2.3 Digital Implementation

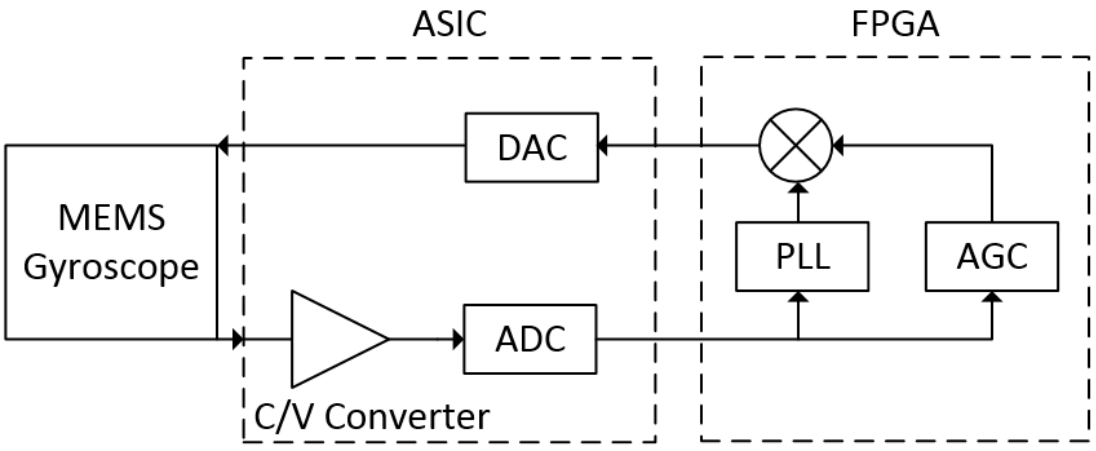

Figure 2.1. Conventional digital drive mode control for MEMS gyroscope.

Digital implementation of gyroscope drive mode control involves converting the analog output of the gyroscope into the digital domain, where it can controlled with various control strategies.

Conventionally, the current-to-voltage converter, ADC and DAC are implemented on an application specific integrated circuit (ASIC) while the digital control strategies are implemented on a field programmable gate array (FPGA), which provides easier tuning of the controllers. A direct digital synthesizer (DDS) can be implemented. The DDS takes the digital output from the AGC and PLL to realize a controlled oscillator which has high precision [19].

In addition, a delta-sigma modulator ($\Delta\sum$) can be used for analog and digital conversion rather than a pipeline ADC. In a pipeline ADC, multiple low-resolution (above 8-bit) flash conversion stages are cascaded in series. The $\Delta\sum$ ADC, however, converts analog signal into bit stream, which reduces the noise in the system that were added to the analog signal. A band-pass sigma-delta ADC applies noise shaping in the modulator to further reduce quantization noise within the useful bandwidth [20].

2.2.4 Analog Implementation

Analog control strategies are typically realized by prototyping on a breadboard, and then designing and fabricating an ASIC. Another option is to use a field programmable analog array (FPAA) [24], which is more cost efficient compared to its digital counterpart, the FPGA.

J. Alvarez et al. presented an analog circuit implementation of a robust control structure with disturbance identification for mechanical systems [15]. It uses analog operational amplifiers to build circuits for a discontinuous observer, a filter and a controller. Although in the paper, the circuit is tested on an industrial 2 DOF robot, it's possible to be implemented on a gyroscope.

2.2.5 Digital and Analog Implementation

In Table 2.1, a list of papers regarding the control of MEMS gyroscopes is compiled. The analog and digital parts of each control system are described. The amplitude noise and frequency stability of their outputs is also listed.

Table 2.1. Table of Papers Concerning Gyroscope Control.

Paper (Year)	Analog Part	Digital Part	Amplitude noise or noise floor	Phase or frequency stability
Digital closed-loop control based on adaptive filter (2010) [19]	ADC and DAC , drive mode of gyro, current/voltage converter	Amplitude and phase separated for respective control (digital PLL and AGC), demodulated by least mean square (on FPGA)	28 ppm in half hour	770 ppm
MEMS gyroscope with control system using a band-pass continuous-time sigma-delta modulator (2010) [20]	N/A	Simulink model with 2 active RC resonator and 2nd order sensing element to form sixth order delta sigma loop	SNR - 100db Noise floor - 90dBV/ $Hz^{1/2}$	N/A
Digitally controlled MEMS gyroscope with 3.2 deg/hr stability (2005) [21]	ΔΣ modulator, charge amplifier, voltage control circuit, recovery circuit on ASIC	Digital counterpart of analogue AGC, feedback detection, output generation (FPGA)	White noise floor - 0.003 $deg/s/Hz^{1/2}$	Allan variance 3.2 deg/hr
A close-loop digitally controlled with Unconstrained ΔΣ Force-feedback (2009) [22]	ΔΣ modulator	Digitally controlled oscillator, amplitude controller, frequency loop filter	Noise floor - 0.025 $deg/s/Hz^{1/2}$,	Less than 0.25 deg/s
Analysis of a microsensor automatic gain control loop (1999) [23]	N/A	Digital AGC	N/A	N/A
Drive mode control for vibrational MEMS gyroscope(2009) [24]	FPAA is used for implementation of ADRC to resonate the drive axis and to stabilize the output	N/A	0.7% of desired amplitude, 1.5 - 1.7% with variation in testing	N/A
An approach for increasing drive-mode bandwidth of MEMS vibratory gyroscopes (2005) [25]	Multiple (eight) resonators with incrementally spaced resonant frequencies in the drive mode	N/A	Maximum gain variation of 17.2%	600Hz frequency operation region
Drive and Sense Interface for Gyroscopes based on Bandpass Sigma-Delta Modulators (2010) [26]	Fourth order ΔΣ modulator	PLL and AGC on FPGA	-60dBFS over 100Hz bandwidth	N/A

2.3 Gyroscope actuation signal noise

A sinusoidal voltage signal with both stable amplitude and frequency is required to achieve a more accurate measurement. Several sources can cause noise in the voltage signal such as the thermal noise [27] caused by random motion of electrons in conductors and flicker's noise in MOSFETs which occur in the interface between the silicon substrate and the gate oxide layer. A model for analyzing the channel noise for MOSFETs based on drain current model is presented in [28].

2.3.1 Parametric Resonance and Noise Squeezing

An alternative to driving a micro cantilever beam directly is to use parametric excitation, which requires a time-periodic variation of the system's impedance (typically stiffness and mass) [29]. Parametric excitation is evident when its excitation frequency is close to twice the natural frequency of the resonator and its amplitude is greater than a threshold value. Prakash et al. described and implemented parametric resonance by using an electronic feedback circuit to excite a microcantilever with a signal proportional to the product of the microcantilever's displacement and a harmonic signal at the frequency twice or close to twice the natural angular frequency of the microcantilever [29]. This parametric excitation allows symmetric amplitude response in the parametric resonance regime without amplitude jumps and restricts hysteresis, resulting in very sharp and well-behaved amplitude peaks for mass sensing applications.

2.3.2 AGC Noise

Automatic gain control feeds back a portion of the input such that the power level of the output signal stays constant regardless of the input. The feedback network is made up of a detector, a differentiator and a buffer stage. The output of buffer goes into an integrator for generating a DC voltage as the gain control. In order to have an effective control, the DC control signal should be a smooth but slowly varying. However, in reality, noise in the form of ripples appearing at the system input will affect the control signal and disturb the gain.

Schachter et al. analyzed a common AGC system with a white Gaussian noise input and the effects of the noise on the gain of the system [30]. Given a random input, it is essential to determine

the parameters of the system such that ripples caused by the input noise will be greatly reduced so that the mean-squared gain of the system would have an almost linear relationship with the power level of the input signal.

Schachter et al. concluded that for both continuous and pulsed operation, the average value of the gain can be made independent of the noise if the detector level is introduced with a properly chosen shift [30]. However, the variance of the gain depends on the noise level. The ripple factor, which is the ratio of the variance of the gain over the square of the average value of the gain depends on the loop gain, the noise level and the ratio of the time constants of the band pass filter at the AGC input and the integrator. The requirement that this ratio remains small even for high noise levels imposes a limit on the value of the loop gain and forces a compromise between the short and long time steadiness of the output level, the dynamic range of the system and the ripple [30].

Overall, AGC has being used in applications where the dynamic response is slow compared with the carrier frequency. In order to reduce to the noise floor of the input signal, a high speed AGC with nearly no ripple is required; therefore, expenses must be made in terms of loop gain and dynamic range.

Chapter 3
Resonant Drive Circuit

3.1 Gyroscope System

The gyroscope system is composed of two components: the mechanical gyroscope and the electrical drive (RLC resonant circuit and a parallel plate capacitor). The resonant drive circuit and the variable capacitor, C_m, of the MEMS gyroscope can be modeled as in Figure 3.1. The input voltage signal, u(t), is an amplitude-modulated (AM) signal with carrier frequency, ω_c, equal to the resonant frequency of the circuit and modulating frequency, ω_m, equal to the natural frequency of the gyroscope drive mode [10-13].

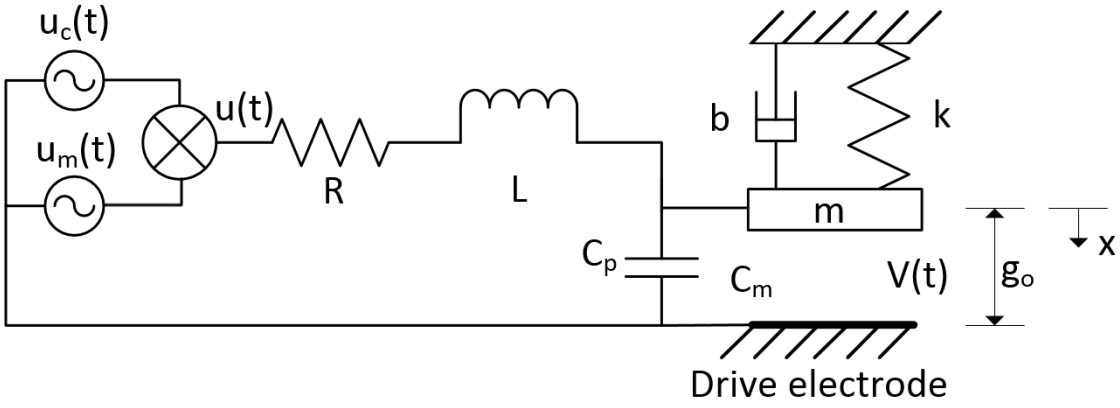

Figure 3.1. Diagram of the MEMS gyroscope, resonant drive circuit and AM input signal.

The mechanical system, Figure 3.1, includes a cantilever microbeam with a flat rectangular proof mass attached to the free end. The suspended mass is excited by a voltage drop V(t) between the proof mass and a fixed electrode made of the time envelope of the modulated signal u(t). When the gyroscope base is rotated about the beam axis (z - direction), Coriolis effect will be introduced in the sense direction (y - direction). This couples the proof mass displacements in the drive and sense directions.

In the drive direction, an electrostatic force is generated between the proof mass and the electrode that is balanced by a mechanical restoring force exerted by the support spring (microcantilever). The uncoupled dynamics of the drive mode can be represented by the spring-mass-damper system,

$$m\ddot{X} + b\dot{X} + kX = \frac{1}{2}\varepsilon A\frac{V^2}{(g_0 - X)^2} \tag{3.1}$$

where X(t) is the displacement of proof mass towards the electrode. The effective mass of the gyroscope is m, the viscous damping coefficient is b and the spring stiffness is k. For the electrostatic force term, **ε** represents the absolute permittivity of air and A represents the area of the electrodes.

The displacement of the proof mass changes the gap distance between the mass and the electrode from an initial value, g_0, which can be related to the parallel plate capacitance C_m by,

$$C_m = \frac{\varepsilon A}{g_0 - X} \tag{3.2}$$

The capacitances will vary inverse proportionally to the change in the gap distance, increasing as the gap becomes smaller.

The RLC circuit, can be described by the equation [10-13],

$$L\ddot{q} + R\dot{q} + \frac{1}{C_p + C_m}q = u(t) \tag{3.3}$$

where C_p represents the parasitic capacitance, q is the total charge of the parallel plate capacitor. Parasitic capacitance is the unwanted capacitance due to close proximity of circuit components. For the MEMS gyroscope, the parasitic capacitance is larger than the capacitance of the parallel plate actuator, C_m. The parallel plate capacitance are in the order of tens of femto-Farads while the parasitic capacitance is in the order of pico-Farads.

Resonant drive circuit actuation eliminates the need of an additional power amplifier by amplifying the input voltage. On the other hand, the actuation voltage should not exceed the pull-in voltage, V_{pi}, of the electrostatic actuator [31],

$$V_{pi} = \sqrt{\frac{8kg_0^3}{27\varepsilon A}} \tag{3.4}$$

to avoid triggering the static pull-in instability between the proof mass and the electrode. The dimensions and material properties of the MEMS gyroscope under study are listed in Table 3.1.

Table 3.1. Parameters of the MEMS Gyroscope [8].

Parameter	***Symbol***	***Value***
Tip Mass	M	3.2 x 10^{-12}kg
Frequency of drive mode	ω_m	13.4kHz
RLC circuit resonant frequency	ω_c	$\omega_m << \omega_c$ ~ 1MHz
Mass per unit length	m_b	1.25 x 10^{-8}kg/m
Pull-in Voltage	V_{pi}	11.26V
Beam length	L_b	400µm
Beam width	w_b	10µm
Beam thickness	t_b	10µm
Initial capacitor gap	g_o	2µm
Density	ρ	2330kg/m^3
Young's modules	E	166GPa

3.2 Amplitude-Modulated (AM) Actuation Signal

The RLC resonant drive circuit is actuated by an amplitude-modulated (AM) signal u(t). This signal is the result of multiplying a carrier wave, $u_c(t)$

$$u_c(t) = u_c sin(\omega_c t) \tag{3.5}$$

with a DC biased modulating signal, $u_m(t)$, which is also referred to as the envelope signal. The frequency of the carrier signal, ω_c, matches the natural frequency of the resonant drive circuit

$$\omega_c = \frac{1}{\sqrt{L(C_p + C_m)}} \tag{3.6}$$

while the frequency of the DC biased modulating signal, ω_m,

$$u_m(t) = u_m sin(\omega_m t) + V_{DC} \tag{3.7}$$

matches the natural frequency of the gyroscope drive mode

$$\omega_{m=} \sqrt{k/m} \tag{3.8}$$

The carrier frequency ω_c is set to a value much greater than the modulating frequency ω_m since the gyroscope is a mechanical resonator acting as a low pass filter. In order to obtain an accurate actuating signal, the higher frequency components should be completely suppressed. This can be achieved by having a carrier frequency as far as possible from the cut-off frequency of this low pass filter.

In addition, a DC bias, V_{DC}, is added to the modulating signal to prevent overmodulation. Therefore, the amplitude modulated signal is obtained by multiplying the carrier signal with the modulating signal:

$$u(t) = V_{DC} u_c sin(\omega_c t) + u_m u_c sin(\omega_m t) sin(\omega_c t) \tag{3.9}$$

Exciting the RLC circuit with an AM signal causes it to resonate at the carrier frequency [10-13], thus amplifying a low input voltage into a higher output voltage, awhile carrying the information in the modulating signal.

3.2.1 Overmodulation and Distortion

In order to avoid overmodulation, the modulating signal must have a DC bias level greater or equal to its peak amplitude. In other words, its minimum peak or trough level should not go below zero. A conventional modulation method is to use the carrier peak amplitude as the bias level such that

$$V_{DC} = u_c \tag{3.10}$$

If that is the case, the amplitude of the carrier signal must be greater than the amplitude of modulating signal, such that the modulation index,

$$m = \frac{u_m}{u_c} \tag{3.11}$$

is between 0 and 1. The effect of varying the modulation index of an AM signal is simulated using

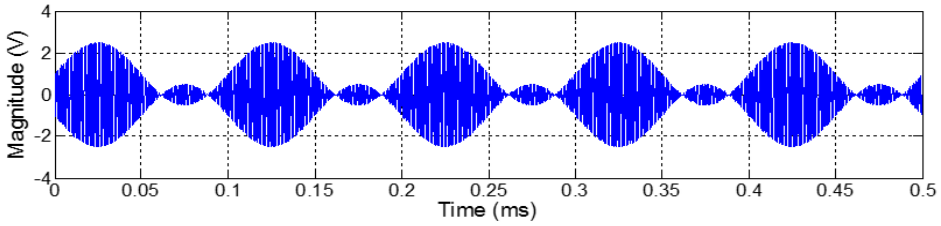

a) m = 1.5

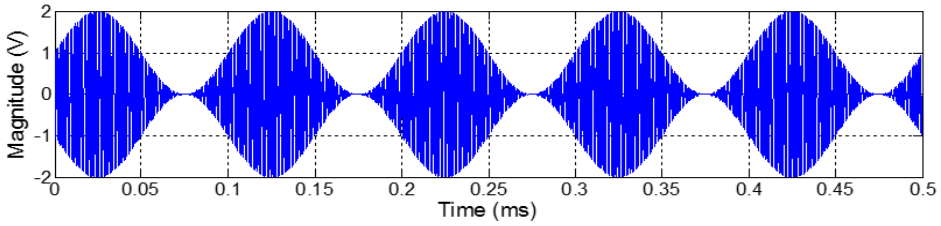

b) m = 1

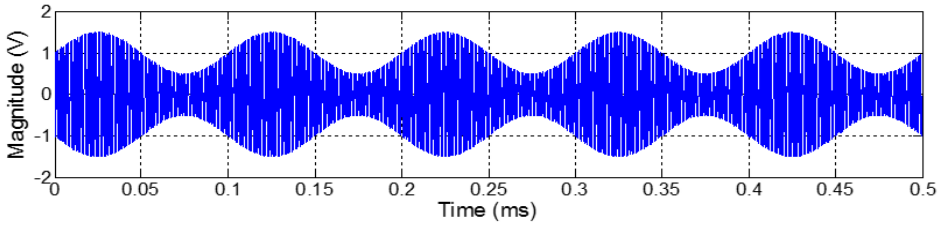

c) m = 0.5

Figure 3.2. The effect of the modulation index on an AM signal.

Matlab, Figure 3.2. The carrier signal is kept constant at a frequency of ω_c = 1 MHz and a peak amplitude of u_c = 1 V. The modulating signal frequency is ω_m = 10 kHz with an offset DC bias of V_{DC} =1 V, while its peak amplitude is varied to obtain different modulation indices.

The distortion of the overall AM signal form can occur because of overmodulation and clipping of the negative peaks, which will create undesired harmonics [32]. These harmonics will modulate with the carrier signal and in turn, generate more sidebands. To prevent distortion, the carrier wave must have a higher amplitude u_c than the modulating signal u_m.

3.3 AM signal in Frequency Spectrum

In order to better analyze the AM signal in frequency domain and investigate potential for controlling it, we rewrite equation 3.9 as:

$$u(t) = u_c\,[V_{DC} sin(\omega_c t) + \frac{u_m}{2}\cos(\omega_c t - \omega_m t) - \frac{u_m}{2}\cos(\omega_c t + \omega_m t)] \qquad (3.12)$$

The AM signal has three components in the frequency domain. The main peak is at the carrier frequency, ω_c. Two additional peaks at (ω_c - ω_m) and (ω_c + ω_m) are also available as a result of AM modulation. They are called the lower sideband (LSB) and the upper sideband (USB), respectively. An AM signal is simulated using Matlab in both time and frequency domain, Figure 3.3. The modulating signal frequency is ω_m = 10 kHz with a peak amplitude of u_m = 1 V, and an offset DC bias of V_{DC} =1 V. The carrier signal has the frequency of ω_c = 1 MHz and peak amplitude of u_c = 1 V.

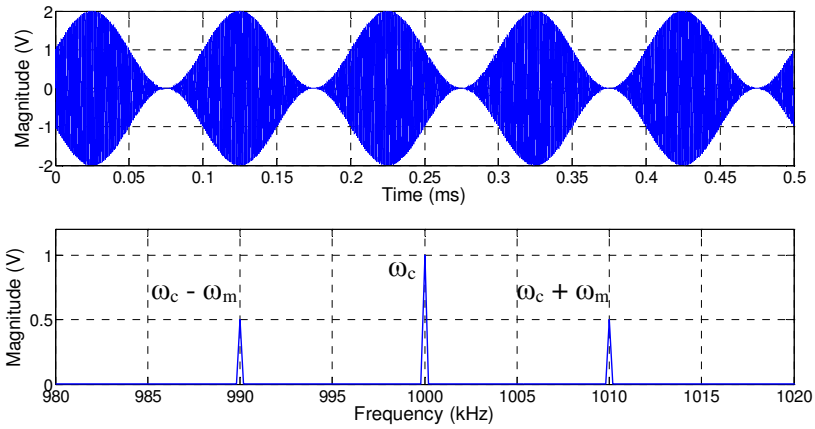

Figure 3.3. A double sideband full carrier (DSB-FC) AM signal in time domain (top) and frequency domain (bottom).

It can be seen from equation 3.12 that the amplitude of the carrier signal, $u_c(t)$, scales the magnitude of the entire signal. The amplitude of the modulating signal, $u_m(t)$, scales the magnitude of both LSB and USB. The DC bias of the modulating signal, V_{dc}, scales the magnitude of the peak at the carrier frequency. This information can be utilized to design control strategies for stabilizing AM signals, which will be discussed in Chapter 5.

The resulting electrostatic force acting on the gyroscope is proportional to the square of the AM signal,

$$F_{es}(t) = \frac{1}{2}\varepsilon A\frac{u^2(t)}{(g_0 - X(t))^2} \tag{3.13}$$

In order to preserve the input power and reduce multi-frequency excitations, the input AM signal can be altered such that it does not include all three frequency components. In our case, four types of input AM signal are considered, depending on which of the three frequency components are included in the signal. The most suitable type of AM signal should be used to excite the resonant drive circuit.

In order to predict the effect each type of AM signal have on the electrostatic force applied to the gyroscope, the square of the signals are graphed in both time and frequency domain, as shown in Figure 3.3 to Figure 3.6.

3.3.1 Double sideband full carrier (DSB-FC)

A double sideband full carrier (DSB-FC) signal includes all three frequency components: (ω_c - ω_m), ω_c, and (ω_c + ω_m). The signal is produced by multiplying the carrier wave with a DC biased modulating signal such that the modulation index is greater than one.

By squaring the AM signal, eight frequency components are generated. The proportionality of the magnitude of these frequency components are of value in estimating the effects of the input signal on the electrostatic force. The relative magnitudes can be seen from both the graph in frequency domain and the equation of the squared signal, where each term represents the respective frequency component and their coefficients can be used to determine the relationship between their magnitudes.

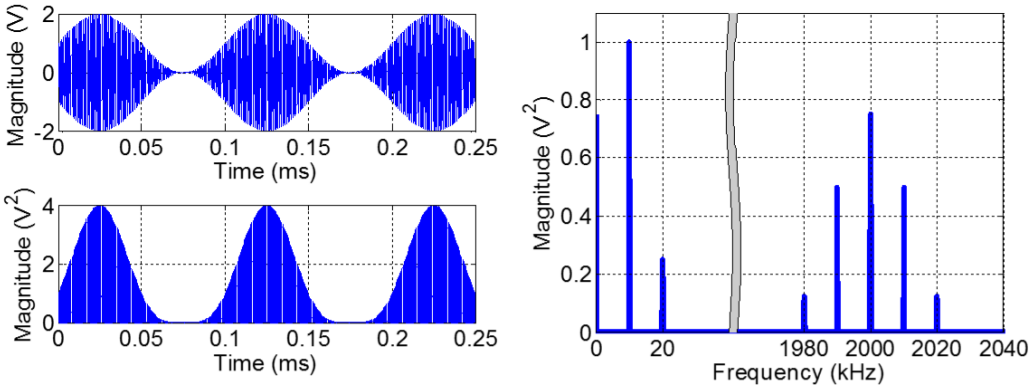

Figure 3.4. The DSB-FC signal in time domain (top left) and the square of the DSB-FC signal in time domain (bottom left) and frequency domain (right).

In this case, the squared DSB-FC signal would be

$$u^2(t) = \frac{{u_c}^2{u_m}^2}{4} + \frac{{V_{DC}}^2 u_c^2}{2} - \left(\frac{{u_c}^2{u_m}^2}{4} + \frac{{V_{DC}}^2{u_c}^2}{2}\right)\cos(2\omega_c t) \tag{3.14}$$
$$- \frac{{u_c}^2{u_m}^2}{4}\cos(2\omega_m t) + \frac{{u_c}^2{u_m}^2}{8}\cos(2\omega_c t - 2\omega_m t)$$
$$+ \frac{{u_c}^2{u_m}^2}{8}\cos(2\omega_c t + 2\omega_m t) + V_{\mathrm{DC}} u_c^2 u_m \sin(\omega_m t)$$
$$+ \frac{V_{\mathrm{DC}} u_c^2 u_m}{2}\sin(2\omega_c t - \omega_m t) - \frac{V_{\mathrm{DC}}{u_c}^2 u_m}{2}\sin(2\omega_c t + \omega_m t)$$

The lower frequency components: DC, ω_m, and $2\omega_m$, are of primary interest as the MEMS gyroscope itself will act as a low pass filter and eliminate the higher frequency components. Both DC voltage and AC voltage at ω_m are required to actuate the gyroscope. A DSS-FC signal contains a relatively large ω_m component which is the primary frequency for exciting the gyroscope. This signal contains a $2\omega_m$ component, which would result in multi-frequency actuation; however, the relative magnitude of the $2\omega_m$ component is small.

3.3.2 Double Sideband Suppressed Carrier (DSB-SC)

A double sideband suppressed carrier (DSB-SC) signal has two frequency components, (ω_c - ω_m) and (ω_c + ω_m), and can be produced by either filtering out the carrier frequency component of a DSB-FC with a sharp notch pass filter or more simply by multiplying the carrier signal with an unbiased modulating signal.

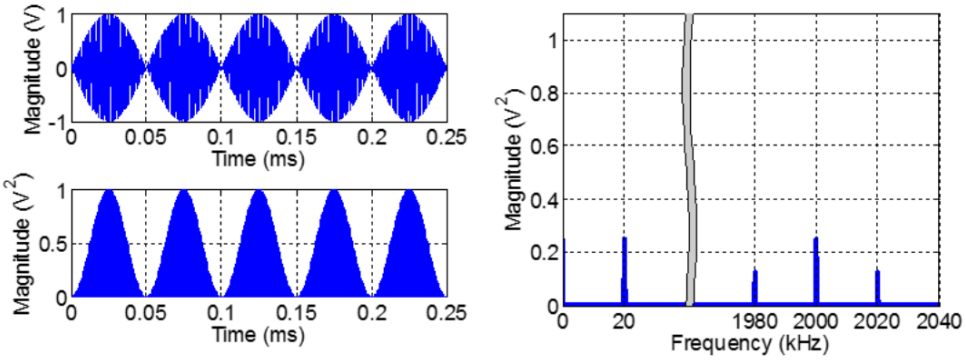

Figure 3.5. The DSB-FC signal in time domain (top left) and the square of the DSB-FC signal in time domain (bottom left) and frequency domain (right).

In this case, the squared DSB-SC signal would be

$$u^2(t) = \frac{{u_c}^2{u_m}^2}{4} + \frac{{u_c}^2{u_m}^2}{8}cos(2\omega_c t - 2\omega_m t) - \frac{{u_c}^2{u_m}^2}{4}\cos(2\omega_m t) - \frac{{u_c}^2{u_m}^2}{4}\cos(2\omega_c t) + \frac{{u_c}^2{u_m}^2}{8}cos(2\omega_c t + 2\omega_m t) \quad (3.15)$$

In the lower frequency spectrum, the squared DSB-SC signal is less viable than the DSB-FC. Specifically for the example signal under study, the DC component drops from 0.75 to 0.25, the component at ω_m disappears and the component at $2\omega_m$ drops from 1 to 0.25.

3.3.3 Single Sideband Full Carrier (SSB-FC)

Either the USB or the LSB of a DSB-FC signal can be filtered out with digital or analog filters to produce a single sideband full carrier (SSB-FC) signal, which contains only the component at carrier frequency and LSB, ω_c and $(\omega_c - \omega_m)$ or at the carrier frequency and the USB, ω_c and $(\omega_c + \omega_m)$.

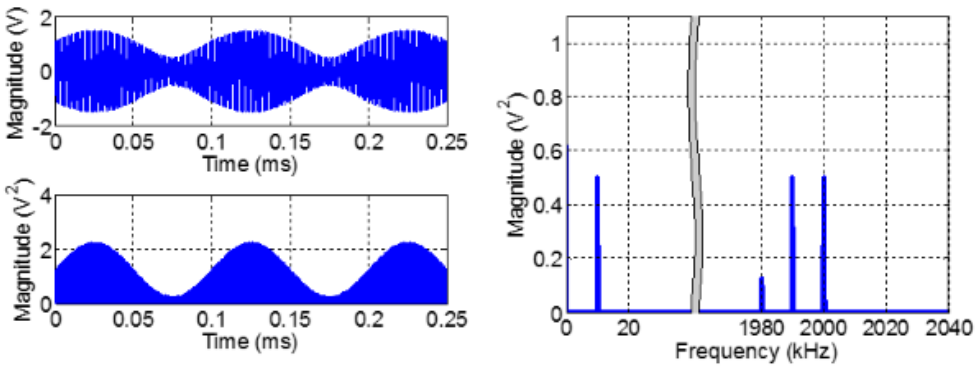

Figure 3.6. The SSB-FC signal in time domain (top left) and the square of the SSB-FC signal in time domain (bottom left) and frequency domain (right).

In this case, the squared SSB-FC signal would be

$$u^2(t) = \left(\frac{{V_{DC}}^2 {u_c}^2}{2} + \frac{{u_c}^2 {u_m}^2}{8}\right) - \frac{{V_{DC}}^2 {u_c}^2}{2} cos(2\omega_c t) + \frac{V_{DC} {u_c}^2 u_m}{2} sin(2\omega_c t - \omega_m t) + \frac{V_{DC} {u_c}^2 u_m}{2} sin(\omega_m t) + \frac{{u_c}^2 {u_m}^2}{8} cos(2\omega_c t - 2\omega_m t) \quad (3.16)$$

In the lower frequency spectrum, the squared SSB-FC signal is more viable than the DSB-SC. Specifically, the DC component raises from 0.25 to 0.625, a signal component appears at ω_m with an amplitude of 0.5 and the component at $2\omega_m$ disappears. While the relative magnitude of the ω_m component is lower than that of a DSB-FC, it has the advantage of not containing the $2\omega_m$ component and therefore avoiding multi-frequency excitation. Specifically, the DC component drops from 0.75 to 0.625, the component at ω_m drops from 1 to 0.5 and the component at $2\omega_m$ disappears.

3.3.4 Single Sideband Suppressed Carrier (SSB-SC)

The single sideband suppressed carrier (SSB-SC) signal has only the LSB (ω_c - ω_m) or the USB component (ω_c + ω_m) and can be produced by filtering out the other frequency components or using modulators such as the Hartley modulator. The effective electrostatic force generated by this type of AM signal does not have the required frequency component ω_m for actuating the gyroscope. Compare to the DSB-FC signal, the DC component drops from 0.75 to 0.125 and both of the frequency components at ω_m and $2\omega_m$ disappear.

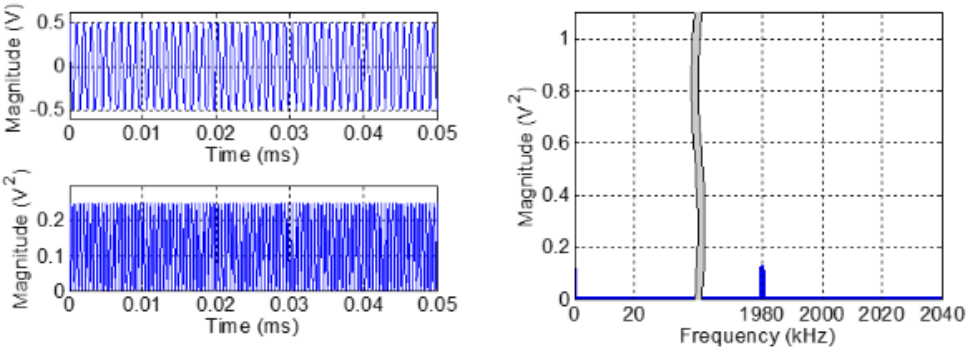

Figure 3.7. The SSB-SC signal in time domain (top left) and the square of the SSB-SC signal in time domain (bottom left) and frequency domain (right).

In this case, the squared SSB-FC signal would be

$$u^2(t) = \frac{{u_c}^2{u_m}^2}{8} + \frac{{u_c}^2{u_m}^2}{8} cos(2\omega_c t - 2\omega_m t) \tag{3.17}$$

3.3.5 Evaluation

After evaluating the effect each of the four AM signal types have on the electrostatic force applied to the gyroscope, we conclude that a single sideband full carrier (SSB-FC) signal would be most suitable for a single frequency excitation. Using a SSB-FC signal to excite the RLC circuit would generate an electrostatic force with the desired components: a DC component and a frequency component at ω_m. We can achieve the SSB-FC signal by filtering out the USB of a DSB-FC signal.

Chapter 4
Automatic Gain Control

4.1 Overall Control Loop

Automatic gain control (AGC) circuits are used in modern applications such as disk drives, hearing aids and communication systems to stabilize the amplitude of signals, especially when the input signals have large dynamic range [35]. Both feedforward and feedback AGC are introduced with an objective of producing a constant output voltage regardless of the change in input voltage.

The overall functional principle behind feedforward and feedback AGC circuits is to proportionally decrease the gain as the input amplitude level increases and vice versa. The signal amplitude level is detected at a point in the circuit and compared to a setpoint voltage level to produce a control signal. The control signal, which should be inversely proportional to the change in the input amplitude, is then used to set the gain of a variable gain amplifier (VGA). The VGA amplifies or attenuates the input signal based on the level of the control signal.

In addition, a signal conditioning circuit can be added, which includes a low pass filter for reducing high frequency noise, AC coupling capacitors for reducing the DC offset and a voltage buffer for providing a low output impedance.

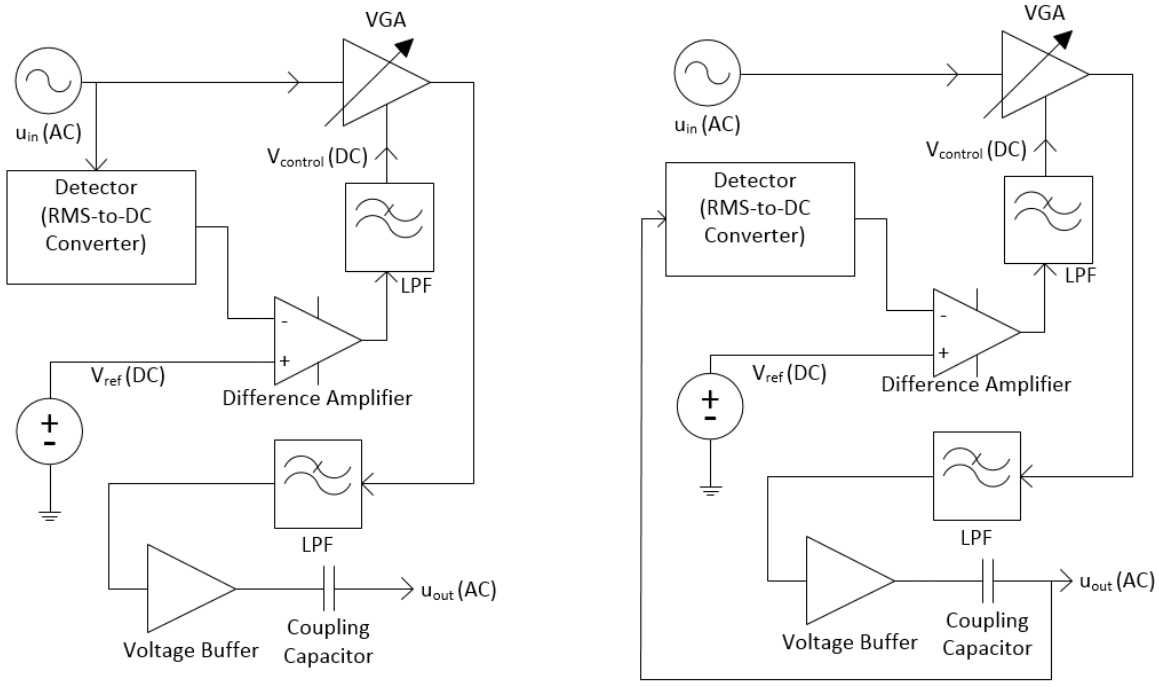

Figure 4.1. A feedforward (left) and a feedback (right) AGC with signal conditioning circuitry.

4.2 Feedfoward AGC

The feedforward AGC, Figure 4.1 (left), extracts a control signal using a detector to compare the input signal, u_{in}, to a reference signal. The control signal is inversely proportional to the error in the input amplitude. In order to protect the signal from higher frequency noise and higher harmonics, the control signal is then passed through a low pass filter called the loop filter. The difference amplifier and the loop filter act as an error integrator, accumulating errors based on the time constant of the loop filter. The VGA then amplifies or attenuates the input signal based on the level of the control signal. The advantage of a feedforward AGC is that it has a faster response time and can avoid instability problems since the time constant only depends on the detector response time, which is much faster than the feedback loop operation [34].

4.3 Feedback AGC

The feedback AGC, Figure 4.1 (right), has similar implementation to the feedforward AGC, except that it compare the output signal, u_{out}, rather than the input signal, to the reference signal. By doing so, it closes the loop on the entire amplification and conditioning circuit. This allows the error integrator to capture the error in the entire circuit up to the feedback point instead of only the input signal error. A feedback AGC must be designed such that its loop can be closed by incorporating a fast VGA. The overall operation is similar to a proportional-integral (PI) controller, where the gain of the difference amplifier is used to tune the proportional controller and the time constant of the low pass filter is used to tune the integral controller.

4.4 Variable Gain Amplifier

The variable gain amplifier (VGA) is the core component of an analog automatic gain control system, the digital equivalent is called a programmable gain amplifier (PGA) [35]. The VGA has two inputs: the AGC input and a slowly varying DC control voltage which adjusts the gain of the output. The most basic VGA can be achieved by simply multiplying the DC control voltage with the AC input using an analog multiplier. There are two types of VGA internal structure. An input VGA (IVGA) has a passive variable attenuator followed by a fixed gain amplifier while an output VGA (OVGA) has a fixed gain amplifier followed by a passive attenuator [34]. A variable gain attenuator can be build using a R-2R ladder network.

In addition, VGA can have either a linear or linear-in-dB relationship between the AGC input and the DC control signal. A linear gain VGA can be implemented by using an analog multiplier,

$$u_{out} = kV_{control}u_{in} \tag{4.1}$$

where k is a proportional gain set by a voltage divider. The advantage of a linear gain VGA is its simple structure since a basic multiplier can be used. However, its disadvantage is that its maximum input level will be limited by the loop gain.

An IVGA have a logarithmic relationship between the input signal and the gain control voltage,

$$u_{out} = k_1(10^{k_2 V_{control}})u_{in} \tag{4.2}$$

This makes it a more popular choice since the maximum input level with low distortion is relatively independent from the gain setting, which is essential for the VGA as the gain would be varying [34].

The VGA should not limit the frequency operation and the linearity of the system. Other parameters that needs to be consider when choosing a VGA are similar to the parameters for any amplifiers. These includes the gain-bandwidth product, slew rate, output noise spectral density and gain accuracy.

4.5 Detector

There are several methods in which the amplitude level of the input or output signal can be detected. The detector does not require a very wide dynamic range since it operates at a constant average level when the AGC loop is in equilibrium. A peak detector outputs the level of the signal peaks. An envelope detector outputs the envelope shape of the signal, similar to the modulating signal of an AM signal. Both the peak detector and envelope detector can be achieved using a simple circuit consisting of a diode, capacitor and a resistor; however with different time constants. Average detector and trough detector are also possible alternatives for biased signals.

An RMS-to-DC converter outputs the root mean square (RMS) level of the signal. For an unbiased sine wave, the RMS level is equal to

$$V_{RMS} = \frac{V_{peak}}{\sqrt{2}} \tag{4.3}$$

where V_{peak} is the peak amplitude of the sine wave. Overall, an RMS-to-DC converter is more flexible in comparison to other type of detectors since its accuracy is maintained regardless of the shape of the input signal. Although it is not required, a detector with a dB output could be used, which would better complement the linear-in-dB response of the VGA.

4.6 Difference Amplifier

The main functionality of the difference amplifier is to subtract the measured detector output from a reference voltage to produce a control signal, which is used to converge the detector output towards the reference voltage. In addition, by subtracting from the reference voltage, the polarity of the control signal is reversed, such that it would decrease as the amplitude of the input signal increases, and vice versa.

The gain of the difference amplifier can be used as a control parameter to calibrate the rate at which the control signal increase or decrease. Since the circuit architecture drive the detector output to converge towards the reference signal, it must use a very stable source to set the reference level. Voltage reference, REF01, is used here since it offers higher accuracy and better temperature stability compared to a power supply.

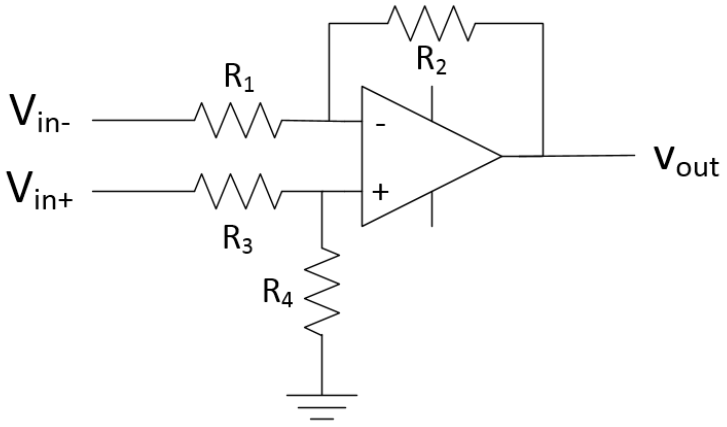

Figure 4.2 Diagram of a difference amplifier.

A classic difference amplifier, Figure 4.2, with an operational amplifier and four resistors is used in differential mode where the two input signal are subtracted and multiplied by a gain which is used as the control parameter. The output voltage is

$$v_{out} = \frac{R_4}{R_3 + R_4}\left(1 + \frac{R_2}{R_1}\right)v_{in+} - \frac{R_2}{R_1}v_{in-} \tag{4.4}$$

The gain of the difference can be controlled since setting the resistor values to

$$R_1 = R_3 \; and \; R_2 = R_4 \tag{4.5}$$

will produce

$$v_{out} = \frac{R_2}{R_1}(v_{in+} - v_{in-}) \tag{4.6}$$

4.7 Filters and Buffers

A simple RC low pass filter can be used as the loop filter, which reduces the ripples of the control signal. Since the RC time constant is normally longer than the AGC closed-loop response time, therefore, the loop filter can be represented by a simple integrator. AC coupling capacitors at the output of the control circuits are used to filter out DC offset noise. Their capacitance are set to small values to avoid creating a second carrier signal. A voltage buffer is utilized to lower the output impedance and increase the output current. In addition, a low pass filter is used at the output of the AGC to eliminate high frequency noise in the output signal. The efficiency of the low pass filter was proven when the frequency spectrum of the signal before and after the filter was obtained using a spectrum analyzer, Keysight N9010A, Figure 4.3. The figure shows a drop in the noise floor of the feedback AGC of about 5 dB.

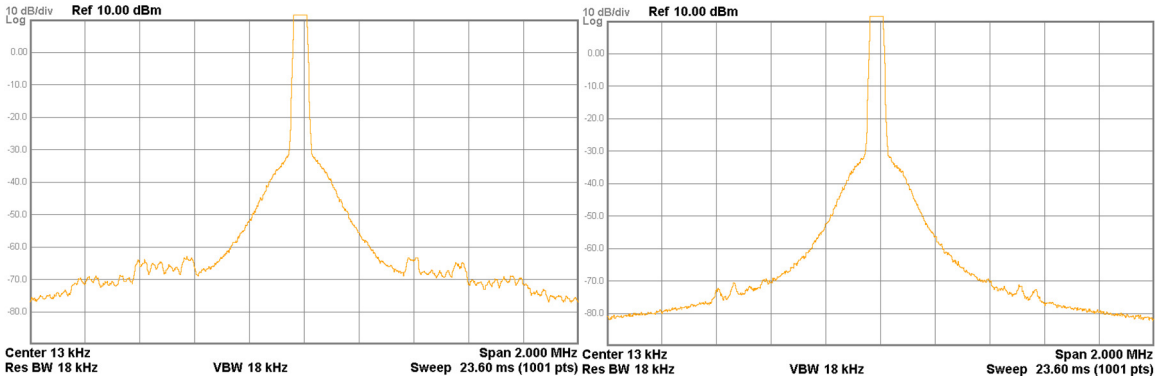

Figure 4.3. FFT of the feedback AGC output before (left) and after (right) the low pass filter obtained from the spectrum analyzer at a center frequency of 13.4 kHz.

4.8 AGC Dynamics

At small input level variations, the general dynamics of an AGC system follow linear theory. However, when a large input signal level variation occurs, the linear AGC theory is no longer accurate and nonlinear theory should be used [33]. The overall AGC system can be described as

$$u_{in} = g(V_{control})u_{out} \tag{4.7}$$

where u_{in} is the input u_{out} is the output, $V_{control}$ is the gain control voltage and $g(V_{control})$ represents the gain control response. The following equation can be used to define $g(V_{control})$ [33]

$$g(V_{control}) = k_1(e^{-k_2 V_{control}}) \tag{4.8}$$

where $k_1 > 0$ and $k_2 > 0$ are constants. A linear in dB response can be represented by

$$g(V_{control})_{dB} = 20\ log_{10}\ g(V_{control}) \tag{4.9}$$

The VGA, AD603, used is linear-in-dB and its gain can be defined as

$$g(V_{control})_{dB} = 40V_{control} + k \tag{4.10}$$

$$g(V_{control}) = 10^{\frac{40V_{control}+k}{20}} \tag{4.11}$$

where $10 < k < 30$ is a variable set by a resistor, which can be used to control the range for the gain. As mentioned above, the loop filter can be represented by a simple integrator. An RMS-to-DC converter, AD737, is used to detect the RMS level of the output signal and can be represented by dividing the peak amplitude of the output signal by the square root of two.

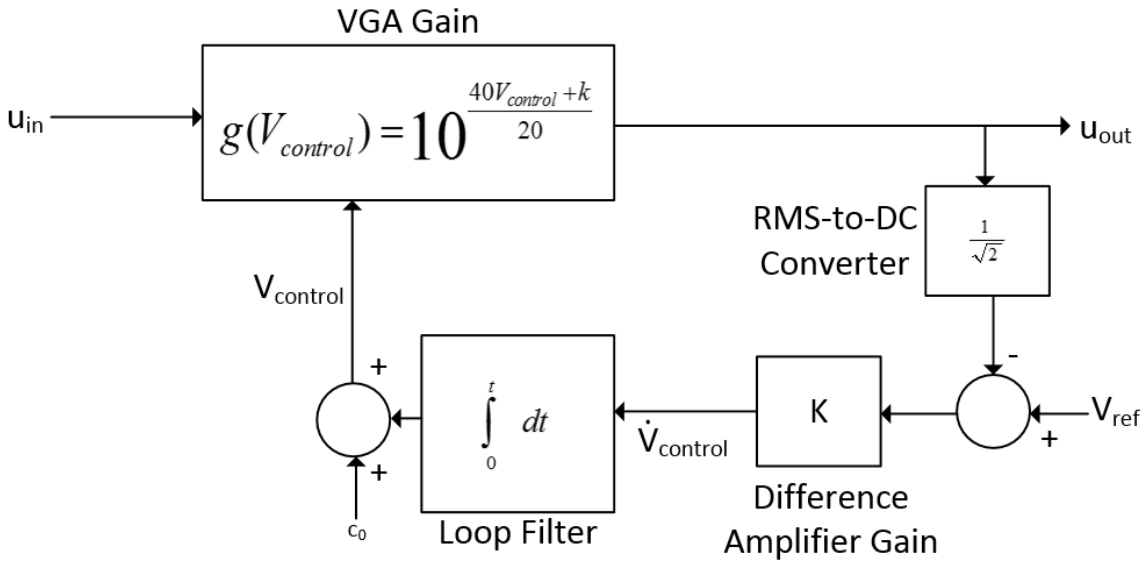

Figure 4.4. Block diagram of a feedback AGC loop.

A model of the feedback AGC loop is presented in Figure 4.4, where k, K and τ, the time constant of the loop filter, can be used as control parameters for settling the input signal RMS towards the reference signal voltage and closing the feedback loop. The analog circuit implementation of the AGC loop is described in Chapter 5.

Chapter 5
Noise Reduction

Feedfack and feedfoward AGC loops are implement on the modulating signal before the resonant drive in order to reduce the signal noise floor. The feedback controller closes the loop on the entire conditioning circuit for the modulating signal while the feedforward controller acts on the input signal to the conditioning circuit. The feedforward and the feedback controllers produce an error signal representing the signal noise by comparing the input and output signals, respectively, with a reference signal.

The actuation circuit is implemented on a breadboard and contains the following modules: an automatic gain control (AGC) loop, an analog multiplier, a low pass filter and a resonant drive circuit. The driving factors in the implementation of the actuation circuit are: noise floor reduction and amplitude stabilization while amplifying the actuation voltage with the resonant drive circuit.

Two possible configurations of the actuation circuit are the control loop excluding the resonant drive circuit and the control loop including the resonant drive circuit. In this chapter, we focus on the first configuration in order to reduce the signal noise entering the resonant drive circuit.

5.1 AGC Loop Response

The AGC loop is implemented at first on a breadboard without the resonant drive circuit. The circuit design implements the feedforward and the feedback AGC circuits shown in Figure 4.1. For the VGA, AD603A is tuned to operate within its linear region by changing the level of the reference signal and the gain of difference amplifier. The VGA has two input signals: a sinusoidal signal, u_{in} and a DC control signal, $V_{control}$. The control signal input for the AD603A has an operating range of ±0.5 V, beyond which the control characteristics are not linear which leads to overall circuit instability. In order to maintain the control signal within its operating range, two Schottky diodes with forward bias voltage of 0.3V are used as limiters by connecting the diodes to the ground in opposite directions to each other. This saturates the control voltage input to the VGA at ±0.3 V.

For the detector, an RMS-to-DC converter is chosen for its flexibility as regards to the different type of signal shapes that can be detected. The AD737 has high accuracy, wide bandwidth and can compute the true RMS value of complex waveform. In order to reduce the noise, the reference signal is obtained a voltage standard rather than the power supply.

To test the AGC, a 13.4 kHz sinusoidal signal was used as the input into the circuit. The output of the AGC stayed constant at 4 Vpp as the input signal varied from 0.8 Vpp to 6 Vpp, Figure 5.1.

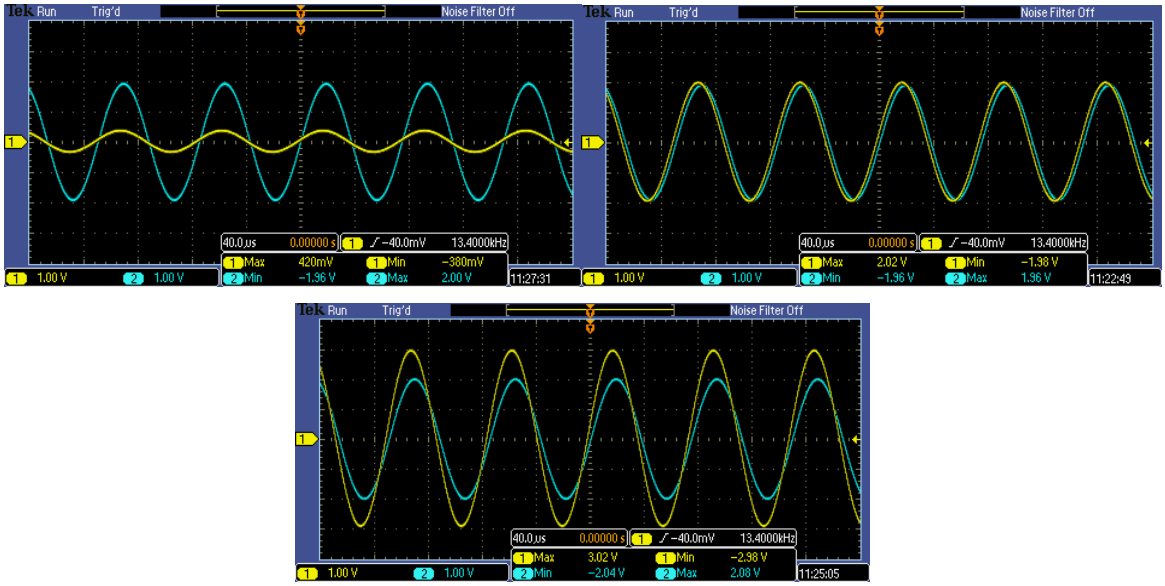

Figure 5.1. The AGC output voltage (blue) when the input voltage (yellow) to the AGC was set at 0.8Vpp, 4 Vpp and 6 Vpp.

5.2 AGC Performance

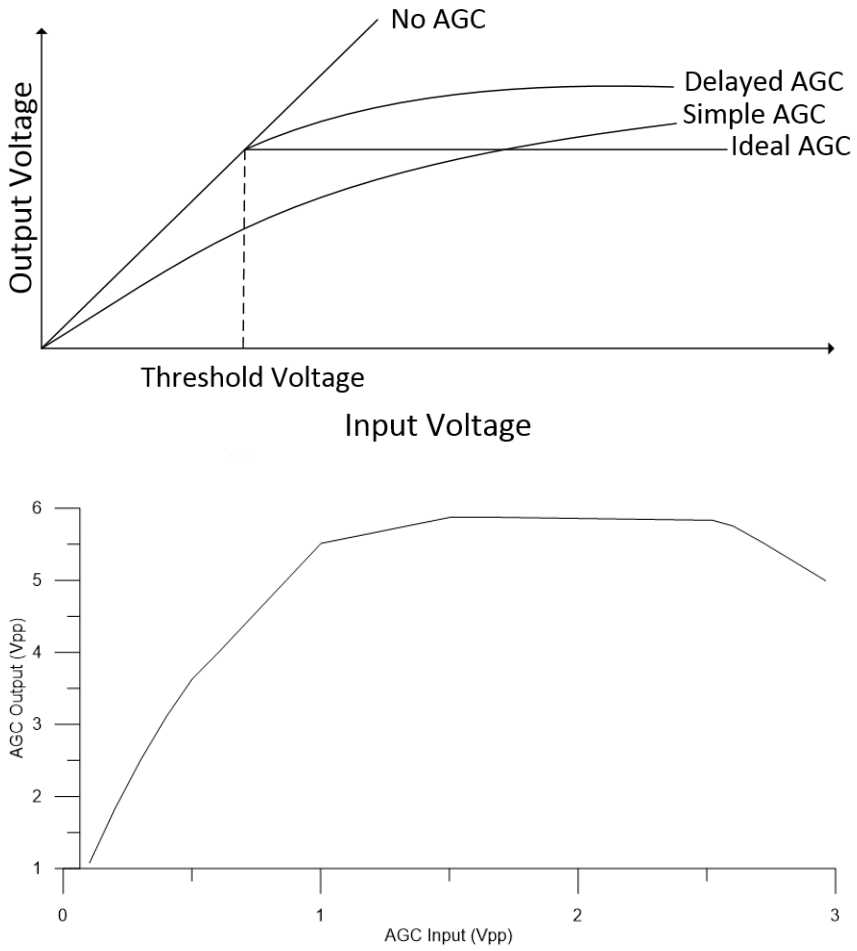

Figure 5.2. Theoretical (top) [36] and measured (bottom) AGC input vs output voltage relationships.

The theoretical input-output voltage relationships of different types of AGC is shown in the top panel of Figure 5.2. The use of a regular amplifier without an AGC circuit architecture will increase the output signal proportionally to the input signal. In the ideal case, an AGC circuit will maintain a constant output signal level above the threshold input voltage level. For small signals below the threshold voltage, the gain of the AGC be constant. However, this is not realistic due to the characteristics of the transistors in a traditional AGC. In a simple AGC, there will be a decrease in the gain regardless of the input signal level, even if a small signal is applied. However, if a delayed AGC

is implemented by applying an adjustable bias, the gain will only be decreased when the desired signal level is reached. After the threshold level, a delayed AGC should have similar or stronger attenuation than a simple AGC.

We measured the input-output voltage relationship of the implemented AGC and found it behaves similar to a delayed AGC with a threshold voltage slightly less than 1 Vpp. The proportional gain of AGC below the threshold voltage was found to be 5.4. The relationship was obtained using an unbiased sinusoidal input voltage. The bottom panel of Figure 5.2 shows the voltage relationship. Furthermore, the proportional decrease of the AGC gain in dB as the input signal level increases can be observed the Figure 5.3.

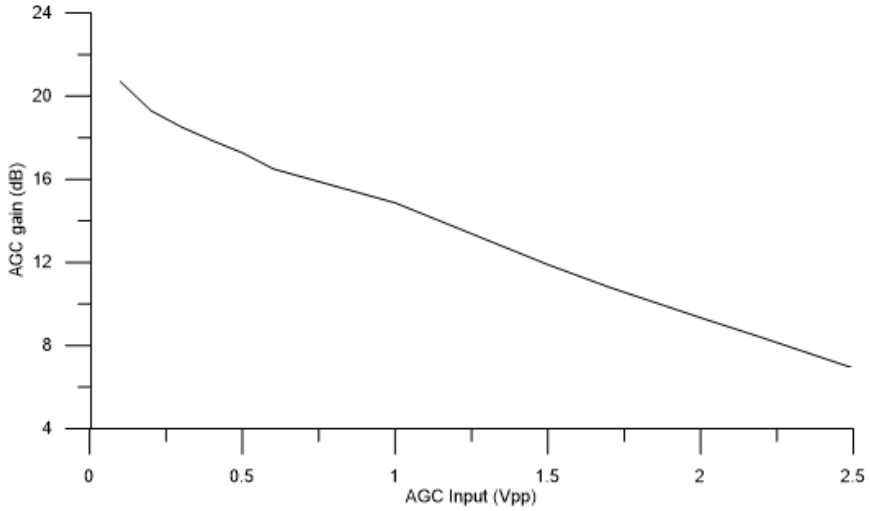

Figure 5.3. AGC gain in dB versus AGC input voltage.

5.3 Noise Floor Comparison

In the overall configuration of the actuation circuit, the AGC loop is used as a conditioning circuit for the modulating signal. The signal is then multiplied by the carrier wave and fed into the resonant drive circuit. A schematic of the actuation circuit is shown is Figure 5.4. The amplitude and frequency of the modulating signal are parameters to be varied for the gyroscope testing. The envelope

signal frequency is set to ω_m = 13.4 kHz and the carrier frequency is set to ω_c = 1 MHz. The output voltage of the AGC loop was found to stay constant for input voltages in the range of 1 Vpp to 6 Vpp.

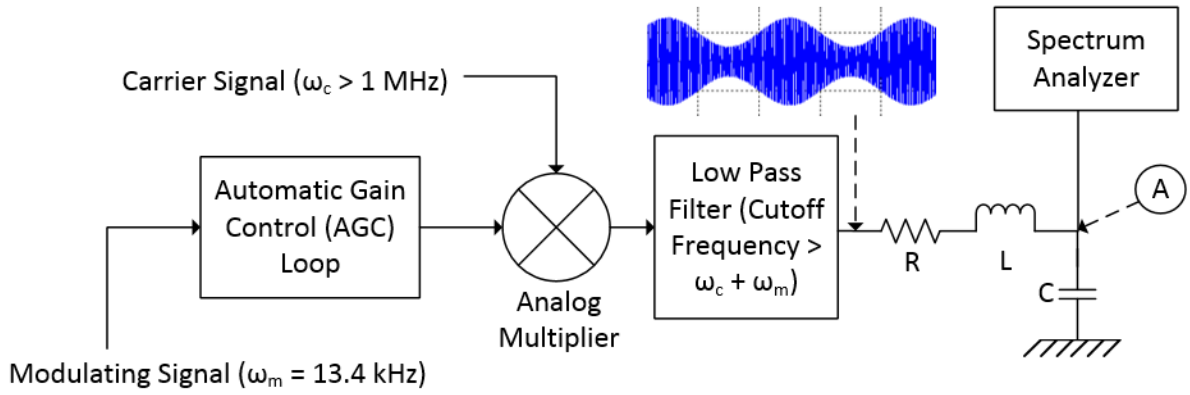

Figure 5.4. A schematic of the signal flow.

We compare the noise floor of the resonant drive circuit output voltage when driven by the feedforward and the feedback configurations of the AGC versus the noise floor in the output when driven by a function generator, BK Precision 4054. A carrier signal from the function generator is multiplied by the modulating signal obtained from all three sources. The generated AM signal is amplified using a resonant drive circuit composed of a 10 nF capacitor and a 1.5 mH inductor. The capacitor represents the combined capacitance of the RLC circuit and the gyroscope.

A spectrum analyzer is used to obtain the frequency spectrum of the amplified modulated signal output of the actuation circuit at the point where it should be fed into the gyroscope, point A in Figure 5.4. The output impedance of the actuation circuit is matched with the input impedance of the spectrum analyzer by utilizing an independent buffer, Figure 5.5.

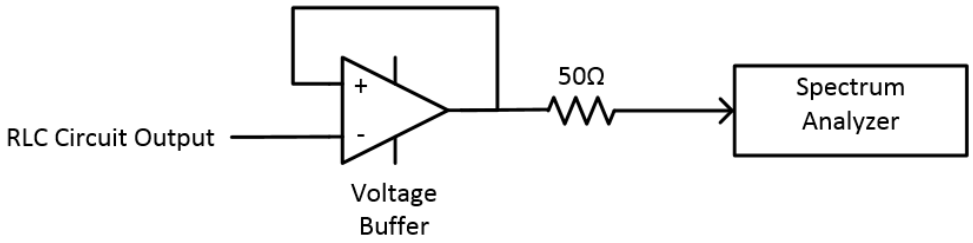

Figure 5.5. An independent voltage buffer for impedance matching between the RLC circuit and the spectrum analyzer.

From the spectrum analyzer, we obtain the ratio of the amplified AM signal's lower sideband power (dBm) to the spectral density of the noise floor (dBm/Hz) averaged over an 8 kHz range. Figure 5.6 shows this ratio in dB/Hz, plotted against the lower sideband power in dBm for all three test case.

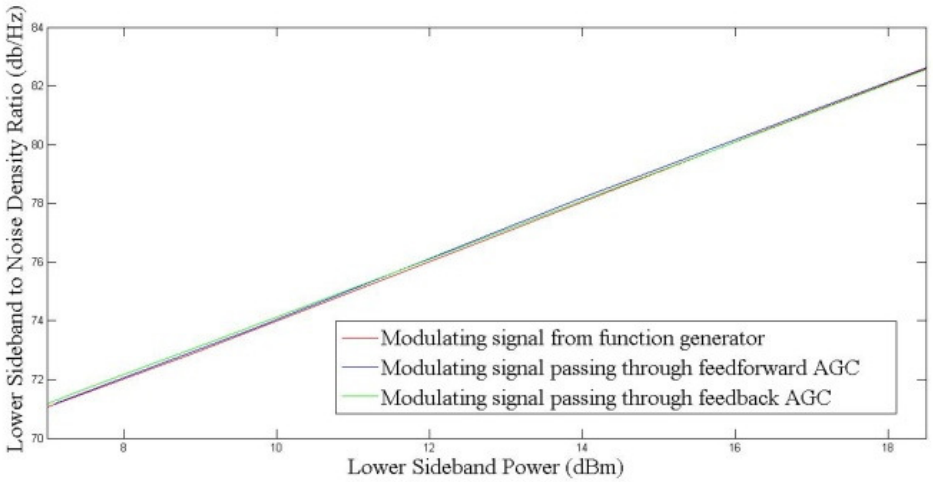

Figure 5.6. Ratio of the lower sideband power (dBm) to noise density (dBm/Hz) of the amplified AM signal where the modulating signals were obtained from the function generator (red), feedforward AGC (blue) and feedback AGC (green) including a 6 dB external attenuation.

The output from the feedforward and feedback AGC circuits have similar signal to noise density ratio compared to that of the function generator, Figure 5.6. The result is reasonable since the

two breadboard AGC circuits are composed of additional through hole IC components, namely the RMS-to-DC converter, the VGA and three extra operational amplifiers, and occupy a large area on the breadboard. These factors give rise to additional thermal and shot noise.

Chapter 6
Amplitude Stabilization

6.1 Control Strategy

The premise behind amplitude stabilization is to apply a control strategy to counter the errors cause by external disturbances such as varying circuit parameters, shifting frequency response and changing temperature. This control loop is especially important for the gyroscope drive mode control since the actuation capacitor acts also as a variable capacitor in the RLC circuit. The displacement of the gyroscope will cause the capacitance to change, which leads to a shifting frequency-response and a gain error vis-a-vis the desired amplitude. The control objective is to provide a single frequency excitation at ω_m that does not change in amplitude as the operating parameters vary. This control strategy would be of value for driving the gyroscope at a fixed operating point and to obtain frequency-response curves that characterize the gyroscope performance.

In addition, a low pass filter is used to suppress the USB of the AM signal for SSB-FC modulation. However, since it is difficult to achieve a low pass filter with a roll-off sharp enough to suppress only the USB, the low pass filter will also affect the magnitude of the LSB and the carrier peaks. A feedback control scheme must be used to stabilize the entire AM signal by stabilizing the bias voltage and by increasing the gain if the amplitude drops and vice versa. Moreover, we must incorporate the resonant drive as the plant within the control loop.

Conventional AGC circuits are designed to keep a sine wave at a constant amplitude. The goal of our control strategy is to stabilize the amplitude and DC bias voltage of the baseband signal. As mentioned in Chapter 4, the three accessible control variables are: the amplitude of the carrier signal, $u_c(t)$, which controls the magnitude of the entire signal; the amplitude of the modulating signal, $u_m(t)$, which controls the magnitude of both LSB and USB; and the DC bias of the modulating signal, V_{dc}, which controls the magnitude of the carrier frequency peak. On the other hand, for a single sideband full carrier (SSB-FC), the magnitude of two peaks at the LSB and the carrier frequency constitute the control objectives. To avoid redundancy, the feedback control should only be applied to two of the

three accessible variables, resulting in the use of two loops to stabilize the signal. However, we know the loops are coupled since feedback information is obtained from the same output AM signal.

Three control schemes are implemented and compared to achieve optimal results. Two control strategies involve controlling the amplitude of the modulating signal and its bias voltage, while the third involves controlling the amplitude of the carrier signal and the bias voltage of the modulating signal. The three control topologies and their results are presented in the following sections.

6.2 Feedback Control Using RMS Detector

The first method of control is relatively simple since it involves using only one RMS detector, AD 637, for controlling both the amplitude of the modulating signal and its bias level, while the carrier signal amplitude is unchanged. The overall control block diagram is shown in Figure 6.1.

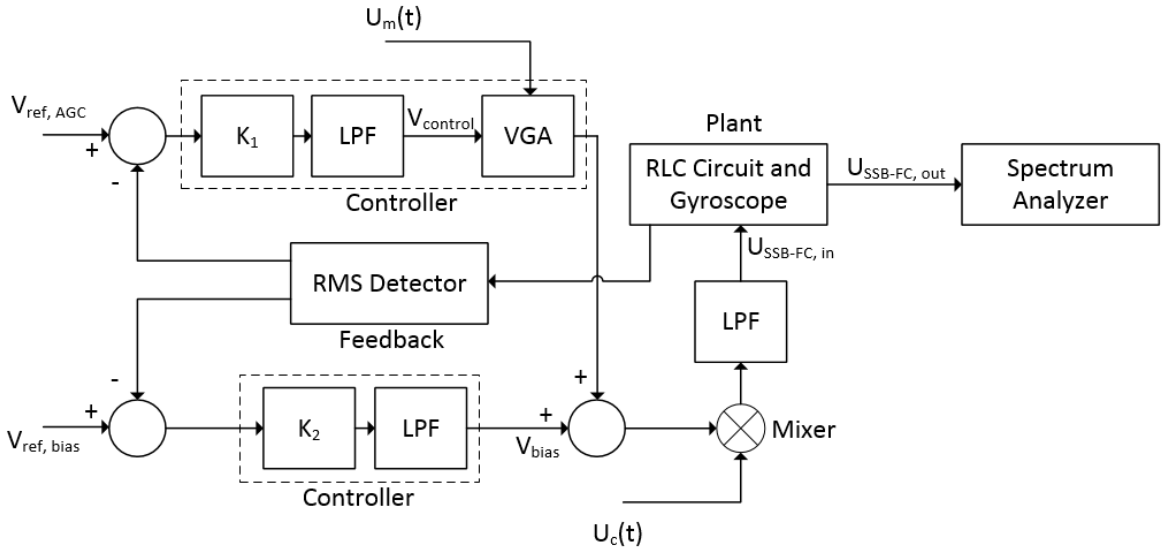

Figure 6.1. Block diagram of the first control scheme.

There are two feedback loops which are coupled since both are using the RMS detector as the feedback signal. The basic premise behind the control scheme is that if RMS level of the output AM signal increases, the control loops will decrease both the input modulating signal amplitude and its bias

level and vice versa. However, the change in the amplitude and the bias level of the modulating signal could be different and therefore need to be controlled by tuning their separate controller gains, K_1 and K_2.

The first feedback loop is similar to an AGC loop and is used for controlling the amplitude of the input modulating signal as discussed in Chapter 4. The output of the RMS detector is subtracted from a reference signal using a difference amplifier to produce an error voltage. The error voltage is multiplied by a gain K_1 to control the variable gain amplifier (VGA), which in turn controls the amplitude of modulating signal. The second loop controls the bias level of the modulating signal by subtracting the output of RMS detector from a second reference level and multiplying by the gain K_2. The first loop outputs an AC signal and the second loop outputs a DC signal. A bias tee circuit is used to add the two signals since it includes a capacitor which allows only the AC signal to pass through and inductor which allows only the DC signal to pass through, Figure 6.2.

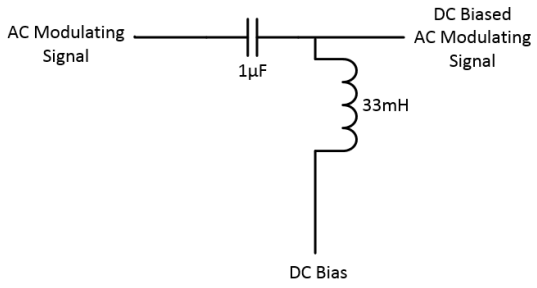

Figure 6.2. Diagram of a bias tee circuit.

An analog multiplier multiplies the resultant biased modulating signal with the carrier signal and a low pass filter filters out the USB of the AM signal to produce the desired SSB-FC signal. Each of the controller gains, K_1 and K_2, is composed of a gain applied by the difference amplifier and a variable gain set by an attenuator (a potentiometer). Furthermore, diode limiter circuits are used to place hard constraints on the control signal such that $V_{control}$ does not exceed the operating range of the VGA, ±500 mV, and V_{bias} does not go below 0 V.

We carry out two experiments to rate the performance of the controller under varying operating conditions. The first experiment involves varying the input carrier signal amplitude and observing variations in output amplitude. The spectrum analyzer is connected in parallel with the RLC capacitor through a buffer. Since the change in carrier signal amplitude will impact the modulating amplitude and the bias level, this is an ideal initial test. For the purpose of testing the control circuit, we use an input carrier frequency of ω_c = 5.64 MHz and a modulating frequency of ω_m = 50 kHz. The results, Figure 6.3, show that the output voltage remains stable as the carrier signal varies from 3 Vpp to 5 Vpp. However, at 2 Vpp, we can see that the LSB peak overshoots by 0.1 V, while the carrier frequency peak undershoots by 0.1 V.

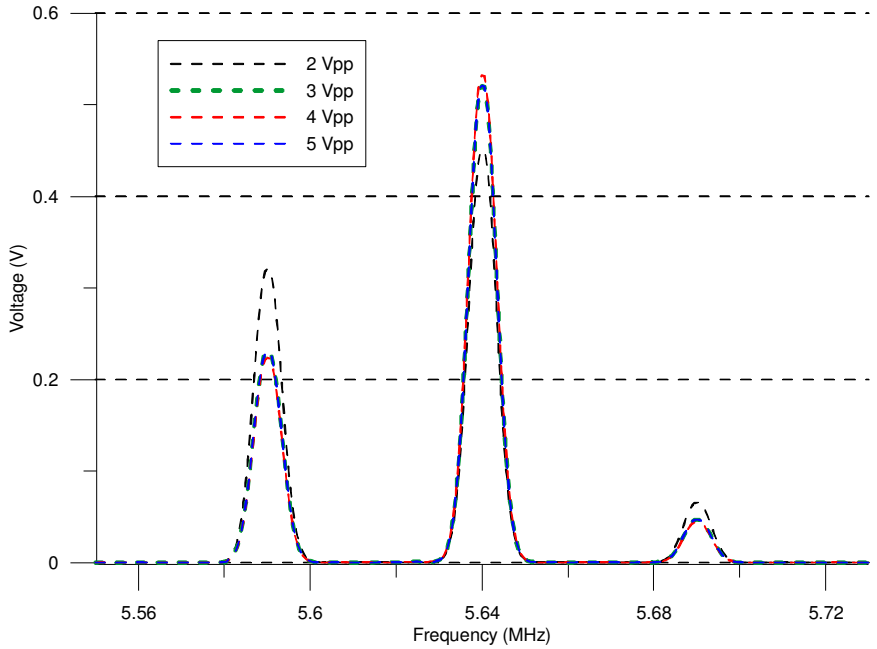

Figure 6.3. Output of the first control scheme in frequency domain as the carrier signal amplitude varies from 2 Vpp to 5 Vpp, as obtained from the spectrum analyzer with 10 dB attenuation.

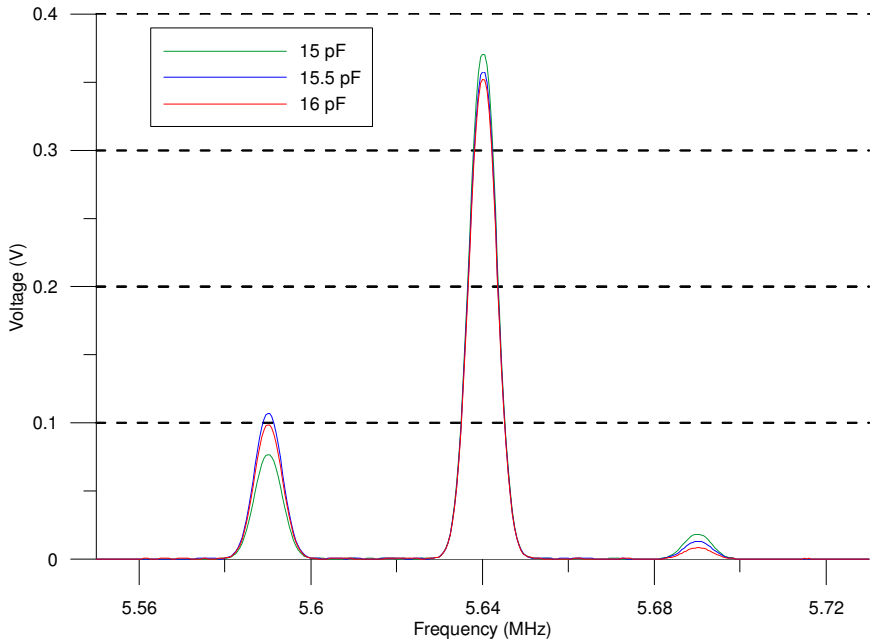

Figure 6.4. Output of the first control scheme in frequency domain with varying capacitance of the resonant drive circuit, as shown on the spectrum analyzer with attenuation.

In the second experiment we varied the capacitance of the RLC circuit to simulate the effect of the gyroscope proof mass displacement with respect to the drive electrode, which causes capacitance change. The capacitance change in the MEMS gyroscope is on the order of tens to hundreds of femtofarads. To be conservative, we applied a change of a picofarad to add a margin of safety to the range of operation. The initial capacitance is set to 15 pF to approximate the combined capacitance of the drive circuit as well as the gyroscope parallel plate capacitor and its parasitics.

The result follows a similar trend as the previous experiment; however, the carrier peak undershoots by 0.02 V, while the LSB peak overshoots by 0.03 V as the capacitance is varied from 15 pF to 16 pF. The drop of the carrier peak is around 9% and the increase at the LSB peak is around 30%. From these experiments, we conclude that the disadvantage of this control scheme is that it does allow a wide operating range for the gyroscope capacitor since both loops depend on one detector. The flaw in this control strategy is that it uses a single detector feedback mechanism, as a result it cannot counteract simultaneous deviations in the two peaks that have opposite directions. From this outcome, we conclude that the use of two separate detectors may improve the controller performance.

6.3 Feedback Using Peak, Trough and Average Detector

The second control scheme is implemented in a similar way to the previous method except for the detection mechanism. The control strategy adjusts the baseband signal amplitude and bias voltage in order to stabilize the peaks at LSB and the carrier frequency against internal (plant parameter variations) and external disturbances. However, instead of using one RMS detector for both feedback loops, separate detectors are implemented, one for each feedback loop.

For the AGC loop, which controls the amplitude of the modulating signal, we feedback the peak to peak amplitude of the output AM signal envelope. This is achieved by first detecting the envelope of output AM signal. The feedback information is obtained by subtracting the trough level of the envelope signal from the overall output signal peak level. This way, the control signal which is fedback is directly related to amplitude of input modulating signal. For the loop which controls the bias level of the modulating signal, we feedback the average level of the output AM signal envelope, which should also be directly proportional to the bias of the input modulating signal.

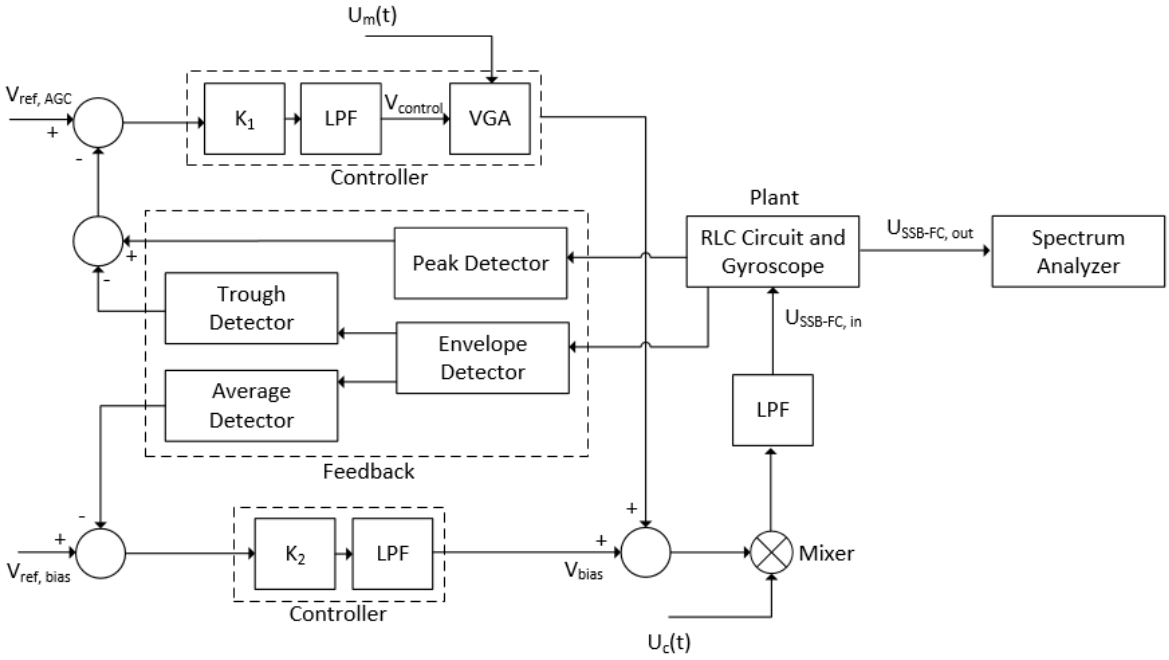

Figure 6.5. Block diagram of the second control scheme.

As with the previous configuration, we perform two experiments on the circuit and observe the outputs from the spectrum analyzer. In the initial experiment, we observe how well the circuit will stabilize the output amplitude with varying input carrier signal amplitude. The output amplitude remains stable if the carrier signal is varied from 3 Vpp to 5 Vpp as with the previous case, Figure 6.6. At 2 Vpp, the carrier peak drops below the desire level by 0.07 V. At 2 Vpp and 3 Vpp, the magnitude of the LSB drops by 0.02 V.

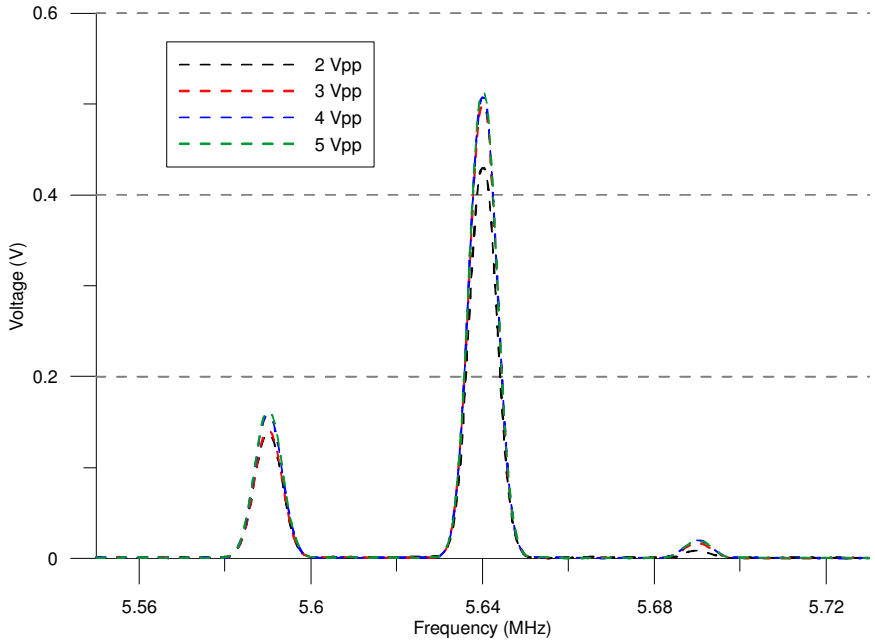

Figure 6.6. Output of the second control scheme in frequency domain with varying input carrier signal amplitude, as shown on the spectrum analyzer with attenuation.

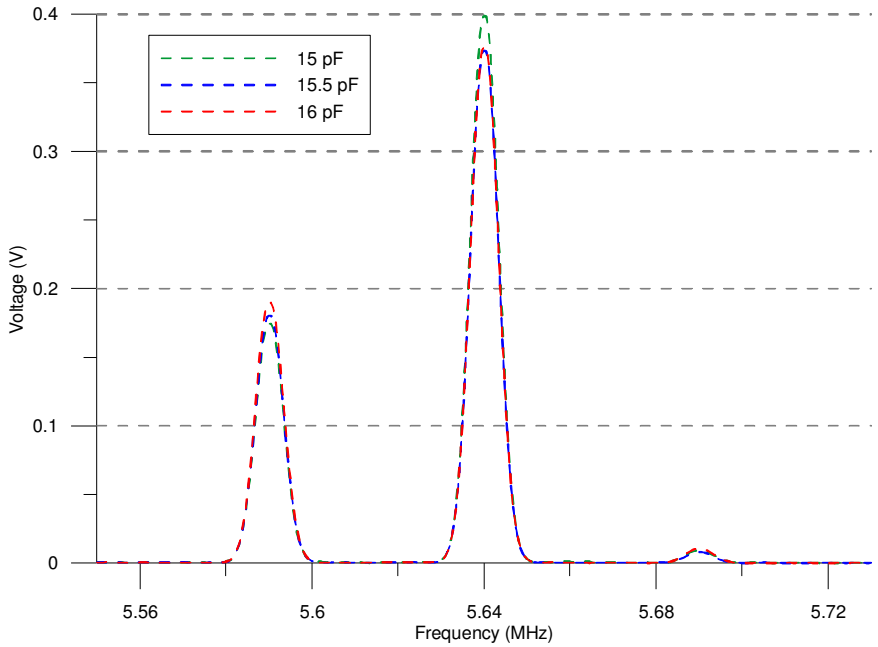

Figure 6.7. Output of the second control scheme in frequency domain with varying capacitance of the resonant drive circuit, as shown on the spectrum analyzer with attenuation.

In the second experiment, as the capacitance is varied from 15 pF to 16 pF, the carrier peak undershoots by around 0.02 V while the LSB peak overshoots by 0.015 V. The drop of the carrier peak is around 6% and the increase at the LSB peak is around 8%. In addition, the magnitude of the LSB remains fairly constant as the capacitance changes. The results from both graphs show that this control scheme has better performance than the previous design, which is at the expense of circuit complexity.

6.4 Feedback Control Using Carrier Amplitude and Bias Level

For the third configuration, the two feedback loops will control the input carrier signal amplitude and the modulating signal bias level without controlling the modulating signal amplitude. The premise behind this method is that the amplitude of the carrier signal will scale the entire signal as seen in Equation 3.12. If the carrier amplitude is controlled, then both the LSB and peak at carrier will scale up and down accordingly.

However, only controlling the carrier amplitude is not enough as there are two control objectives if the frequencies are kept constant. A change in the capacitance of the RLC circuit may not scale both the LSB and the carrier peak the same way that a change in input carrier signal amplitude will scale them due to the RLC frequency response curve. As the frequency response of the RLC circuit shifts, it will not apply the same gain change to both the LSB and carrier peak, but a change in the input carrier signal amplitude will apply the same gain.

This implies that we must take another control parameter into account, either the modulating signal amplitude or its bias level. Controlling the modulating signal amplitude would increase the circuit complexity since a second AGC would be required, whereas controlling the bias level of the modulating signal would be a more effective design. For the AGC loop controlling the carrier signal amplitude, we use an RMS detector as feedback. For controlling the bias level of the modulating signal, we feedback the average of output AM signal's envelope as with the previous configuration.

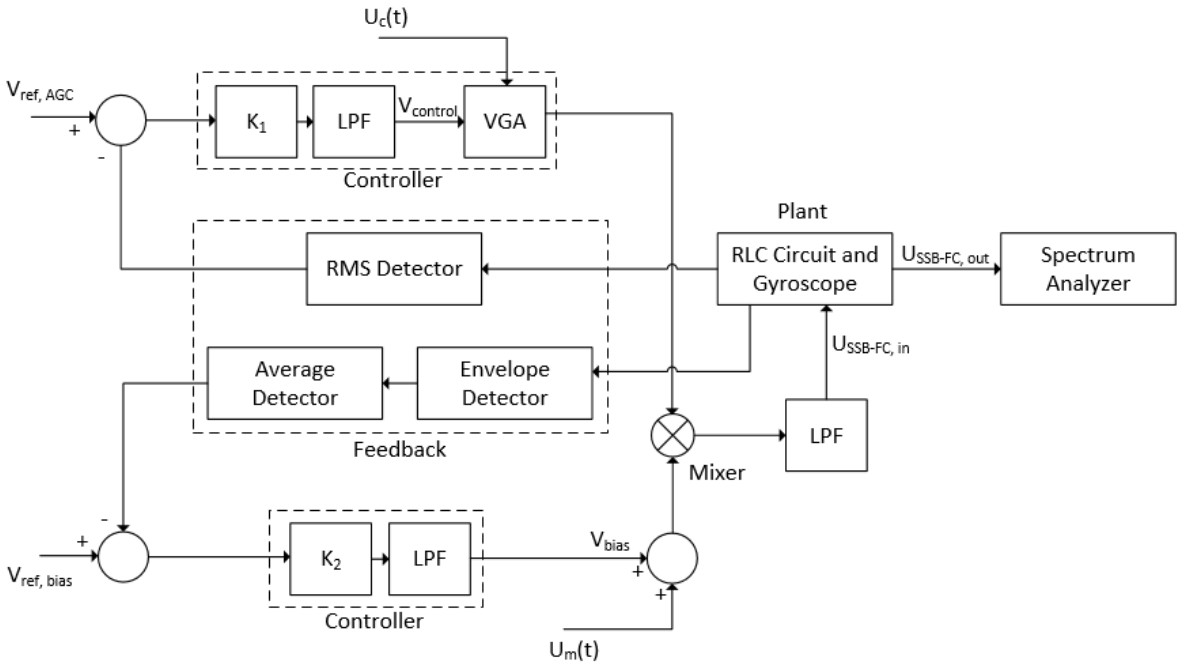

Figure 6.8. Block diagram of the third control scheme.

As with previous control scheme, the circuit is experimented under two conditions: varying input carrier signal amplitude and varying capacitance of the RLC circuit. The results from the spectrum analyzer show the improved performance in comparison to the previous two configurations, Figure 6.9. The output amplitude remains constant as the carrier signal is varied from 1 Vpp to 5 Vpp, demonstrating that the control circuit has a wider operating range than the previous circuits.

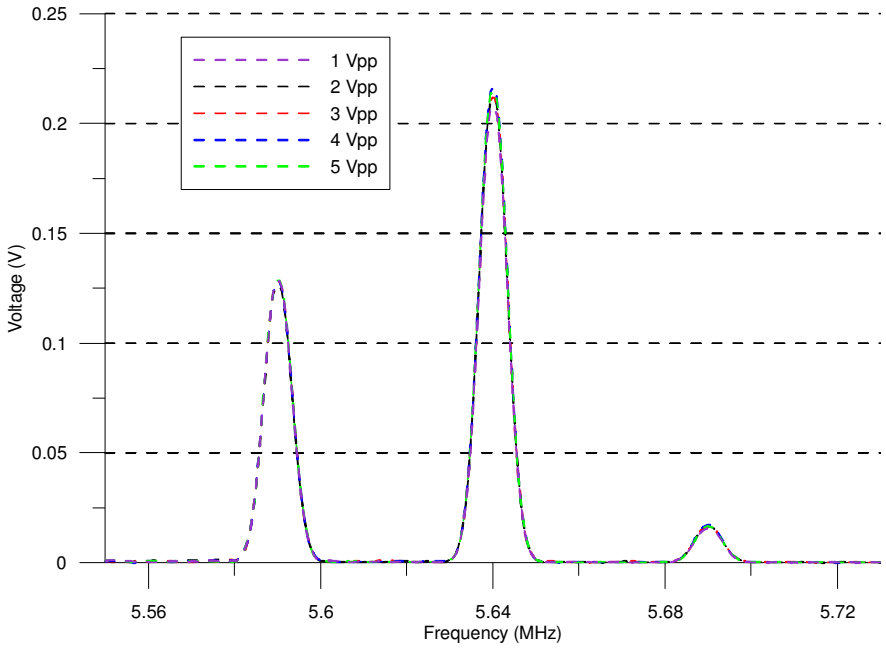

Figure 6.9. Output of the third control scheme in frequency domain with varying input carrier signal amplitude, as shown on the spectrum analyzer with attenuation.

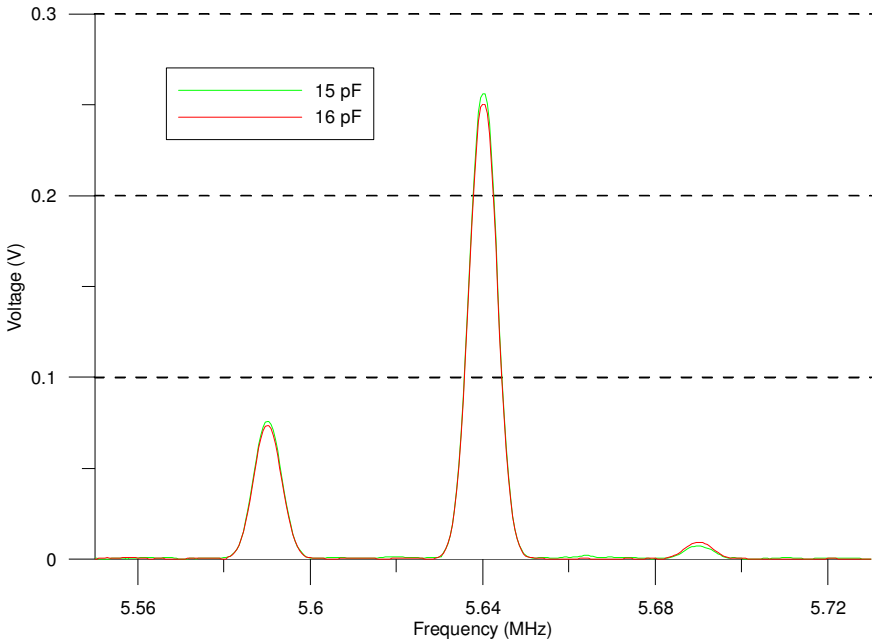

Figure 6.10. Output of the third control scheme in frequency domain with varying capacitance of the resonant drive circuit, as shown on the spectrum analyzer with attenuation.

In addition, the third control scheme performs better at stabilizing the output AM signal as the capacitance of the RLC circuit is changed, Figure 6.10. As the capacitance is varied from 15 pF to 16 pF, the carrier peak undershoots by around 0.005 V while the LSB peak undershoots by 0.001 V. The drop of the carrier peak is around 2% while the drop of the LSB peak is around 1%. This improved performance compared to the previous control scheme is the result of stabilizing the carrier signal instead of the modulating signal. In addition, utilizing an RMS detector instead of additional op amps and external capacitors will reduce thermal and shot noise. The slight deviation of the LSB and carrier peaks from 15 pF to16 pF are in the same direction and have similar gains, suggesting that to improve the performance further, we can use more precise resistors for tuning K_1.

Chapter 7
Conclusions and Future Work

7.1 Conclusions

The electrostatic actuation of a MEMS gyroscope requires a high voltage and stable input signal. Conventionally, a charge pump or an amplifier circuit lowers the input voltage requirement and a feedback control scheme in either analog or digital domain stabilizes the sinusoidal input signal. To fulfill these requirements, we instead develop a breadboard prototype of a single-harmonic amplitude-stabilized resonant drive circuit, which is actuated using a SSB-FC signal. The SSB-FC is generated by multiplying a modulating signal, u_m, with a carrier signal, u_c, and filtering the USB of the resultant AM signal. Using the SSB-FC signal to excite the resonant circuit would generate an electrostatic force oscillating at the natural frequency of the gyroscope along with a DC component. In addition, we design and test an analog control scheme for stabilizing the amplitude of the SSB-FC signal.

Initially, we study the effect of adding a feedback or a feedforward control loop (AGC) to the actuation circuit in attempt to lower the noise floor. The control signals used in both configurations represent the signal noise by comparing the input and output signal, respectively, with a reference signal. However, we find that the breadboard circuit implementations of such control strategies perform similar to a baseline function generator due to additional noise input from the breadboard and the additional components used to implement the controller, such as the amplifiers.

However, a feedback control loop is still required to stabilize the actuation signal. Since the capacitance of RLC circuit depends on the gap distance between the gyroscope parallel plates, it will change due to the vibration of the gyroscope. This variation in capacitance will shift the frequency response of the RLC circuit such that the oscillation will no longer be at the peak of the resonance, resulting in lower signal amplitude. In addition, the low pass filter for the SSB-FC signal will also affect the magnitude of the LSB and the frequency component at the carrier.

In order to avoid changing the gyroscope actuation signal amplitude to an undesired level, different feedback control schemes are implemented for stabilization. The first control scheme uses

only an RMS detector as the feedback to control both the amplitude of the modulating signal and its bias level. The second control scheme uses the difference between the peak and the trough level of the output SSB-FC signal's envelope to control the input modulating signal and the average level of the output signal's envelope to control the bias level of the input modulating signal. The third control scheme controls the amplitude of the input carrier signal with an RMS detector and the bias of the modulating signal with the average level of the output signal's envelope.

By comparison, the last control scheme performs the best in stabilizing the actuation signal, with a carrier peak drop of around 2% as the capacitance is varied from 15 pF to 16 pF, as oppose to 9% and 6% from the first and second control schemes. In addition, the implemented controllers will allow us to perform frequency sweeps for the gyroscope, in which the magnitude of the excitation force is kept constant while its frequency varies. However, the controllers will not allow us to perform force sweeps, which require varying the magnitude of the excitation force.

7.2 Future Work

Continuation of the research includes testing the circuit on a MEMS parallel plate actuator and the frequency modulated MEMS gyroscope which is currently under fabrication. In addition, in order to utilize the resonant circuit to its maximum value, the feedback detection circuitry should be design to withstand a higher voltage. Any voltage limitation on the feedback circuit would restrict the amplification from the RLC circuit regardless of its quality factor.

In addition, the primary aim of the control circuit is to stabilize the amplitude of the actuation signal, which will fluctuate more than its frequency. However, a phase-lock loop (PLL) can be added in conjunction to the AGC for phase and frequency stabilization.

Furthermore, a digital actuation scheme with the same control topology or a different control topology can also be design and implement to compare with the noise floor of the current design.

Next, the actuation circuitry can be implemented on a PCB board to study the effect on the actuation signal noise level. Eventually, it should be design as one chip to be fabricated using bulk integrated circuit (IC) techniques to compliment the MEMS gyroscope.

As a final experiment, the noise level floor the actuation circuit can be compared with the dominant noise of the mechanical gyroscope, thermal noise. If the actuation circuit has a higher noise floor, improvements are required.

Appendix A - Final Actuation Circuit Test Setup

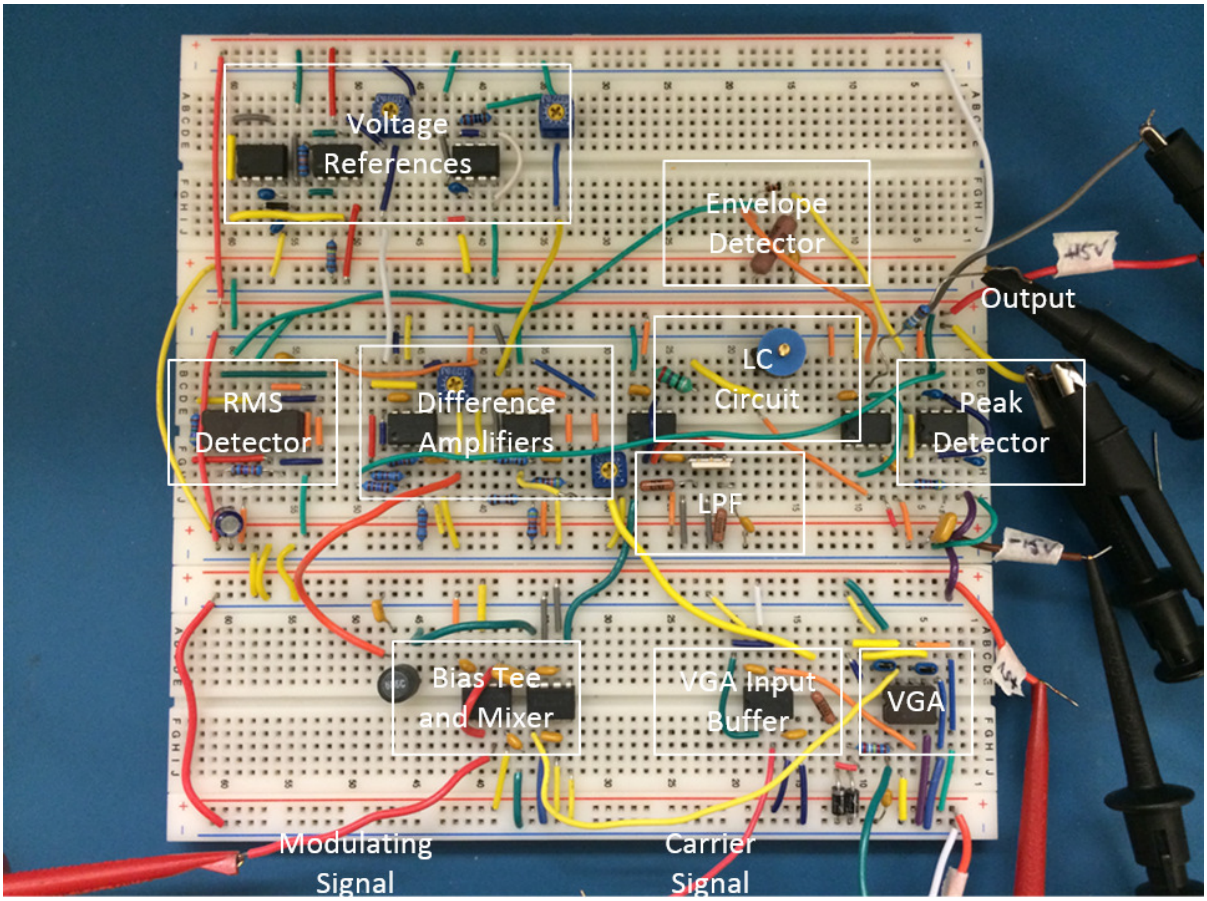

Figure A.1. Test setup of the actuation circuit incorporating the third control scheme.

Bibliography

[1] M. Esashi, T. Ono, “Application Oriented Micro-Nano Electro Mechanical Systems”, *Microprocesses and Nanotechnology, 2007 Digest of papers*, pp. 480-481, 5-8 Nov. 2007

[2] A. A. Seshia, Integrated micromechanical resonant sensors for inertial measurement systems, PhD Dissertation, University of California, Berkeley, 2002.

[3] N. Yazdi, F. Ayazi, K. Najafi, "Micromachined inertial sensors", *Proceedings of the IEEE*, vol.86, no.8, pp.1640,1659, Aug 1998

[4] F. Ayazi and K. Najafi, “Design and fabrication of a high performance polysilicon vibrating ring gyroscope,” in *Proc. IEEE Micro Electro Mechanical Systems Workshop (MEMS’98),* Heidelberg, Germany, Feb. 1998, pp. 621–626.

[5] M. Weinberg, J. Bernstein, S. Cho, A. T. King, A. Kourepenis, P. Ward, and J. Sohn, “A micromachined comb-drive tuning fork gyroscope for commercial applications,” in *Proc. Sensor Expo,* Cleveland, OH, 1994, pp. 187–193.

[6] T. Juneau, A. P. Pisano, and J. H. Smith, “Dual axis operation of a micromachined rate gyroscope,” in *Tech. Dig. 9th Int. Conf. Solid-State Sensors and Actuators (Transducers’97),* Chicago, IL, June 1997, pp. 883–886.

[7] K. Y. Park, C. W. Lee, Y. S. Oh, and Y. H. Cho, “Laterally oscillated and force-balanced micro vibratory rate gyroscope supported by fish hook shape springs,” in *Proc. IEEE Micro Electro Mechanical Systems Workshop (MEMS’97),* Japan, 1997, pp. 494–499.

[8] D. M. Effa, E. M. Abdel-Rahman, and M. Yavuz, “Cantilever Beam Microgyroscope Based on Frequency Modulation”, IEEE/ASME International Conference on Advanced Intelligent Mechatronics: AIM 2013, Wollongong, Australia, July 2013, pp. 844-849.

[9] H. Weinberg, “Gyro Mechanical Performance: The Most Important Parameter”, Analog Devices, MS-2158, 2011

[10] S. Park, E. Abdel-Rahman, M. Khater, "Low Voltage Electrostatic Actuation for MEMS Actuator Using frequency Modulation", ASME IDETC, Portland, OR, August 2013, DETC2013-13376.

[11] S. Park, Y. Bai, John T.W. Yeow, "Design and Analysis of Resonant Drive Circuit for Electrostatic Actuators", IEEE International Symposium on Optomechatronic Technologies (ISOT), Vol 10, pp 1-6, 2010.

[12] S. Park, E. Abdel-Rahman, "Stabilization of Electrostatic Actuators Through Variable Gain Amplifier", ASME IDETC, Chicago, IL, August 2012, DETC2012-71274.

[13] S. Park, “Low Voltage Electrostatic Actuation and Displacement Measurement through Resonant Drive Circuit”, PhD Thesis, University of Waterloo, Waterloo, 2011

[14] A. M. Shkel, R. Horowitz, A. A. Seshia, S. Park, R. T. Howe, “Dynamics and Control of Micromachined Gyroscopes”, Proceedings of the American Control Conference, San Diego, California, June 1999, pp. 2119-2124

[15] J. Alvarez, D. Rosas, J. Pena, "Analog Implementation of a Robust Control Strategy for Mechanical Systems”, *IEEE Transactions on Industrial Electronics*, vol.56, no.9, pp.3377-3385, Sept. 2009

[16] C. Patel, P. McCluskey, "Modeling and simulation of the MEMS vibratory gyroscope”, *2012 13th IEEE Intersociety Conference on Thermal and Thermomechanical Phenomena in Electronic Systems (ITherm)*, pp.928,933, May 30 2012-June 1 2012

[17] L. Aaltonen, K.A.I. Halonen, "An analog drive loop for a capacitive MEMS gyroscope", Analog Integrated Circuits and Signal Processing, Vol. 63, No. 3, pp. 465-476, 2010.

[18] Q. Zheng, L. Dong, D.H. Lee, Z. Gao, "Active Disturbance Rejection Control for MEMS Gyroscopes", *IEEE Transactions on Control Systems Technology*, Vol. 17, No. 6, pp. 1432-1438, 2009.

[19] D. Liu, N.N. Lu, J. Cui, L.T. Lin, H.T. Ding, Z. C. Yang, Y.L. Hao, G. Yan, "Digital closed-loop control based on adaptive filter for drive mode of a MEMS gyroscope”, *Sensors, 2010 IEEE*, pp.1722-1726, 1-4 Nov. 2010

[20] H.T. Ding, Z.C. Yang, G.Z. Yan, M. Kraft, R. Wilcock, "MEMS gyroscope control system using a band-pass continuous-time sigma-delta modulator", *Sensors, 2010 IEEE*, pp.868-872, 1-4 Nov. 2010

[21] H. Rodjegard, D. Sandstrom, P. Pelin, N. Hedenstierna, D. Eckerbert, G.I. Andersson, "A digitally controlled MEMS gyroscope with 3.2 deg/hr stability”, *The 13th International Conference on Solid-State Sensors, Actuators and Microsystems, 2005.*

Digest of Technical Papers. TRANSDUCERS '05, vol.1, pp.535-538 Vol. 1, 5-9 June 2005

[22] J. Raman, E. Cretu, P. Rombouts, L. Weyten, "A Closed-Loop Digitally Controlled MEMS Gyroscope With Unconstrained Sigma-Delta Force-Feedback", *Sensors Journal, IEEE*, vol.9, no.3, pp.297-305, March 2009

[23] R.T. M'Closkey, A. Vakakis, "Analysis of a microsensor automatic gain control loop", *American Control Conference, 1999. Proceedings of the 1999*, vol.5, pp.3307-3311 vol.5, 1999

[24] L. Dong, D. Avanesian, "Drive-Mode Control for Vibrational MEMS Gyroscopes", *IEEE Transactions on Industrial Electronics*, vol.56, no.4, pp.956-963, April 2009

[25] C. Acar, A.M. Shkel, "An approach for increasing drive-mode bandwidth of MEMS vibratory gyroscopes", *Journal of Microelectromechanical Systems*, vol.14, no.3, pp.520-528, June 2005

[26] T. Northemann, M. Maurer, S. Rombach, A. Buhmann, Y. Manoli, "Drive and sense interface for gyroscopes based on bandpass sigma-delta modulators", *Proceedings of 2010 IEEE International Symposium on Circuits and Systems (ISCAS)*, pp.3264-3267, May 30 2010-June 2 2010

[27] R. P. Leland, "Mechanical-Thermal Noise in MEMS Gyroscopes", *IEEE Sensors Journal*, Vol. 5, No. 3, pp 493-500, 2005.

[28] S. Asgaran, M.J. Deen, C.H. Chen, "Analytical Modeling of MOSFET Noise Parameters for Analog and RF Applications," *IEEE Custom Integrated Circuits Conference*, Vol. 17, No. 4, 2004.

[29] G. Prakash, A. Raman, J. Rhoads, R. G. Reifenberger, "Parametric noise squeezing and parametric resonance of microcantilevers in air and liquid environments", *Review of Scientific Instruments* , vol.83, no.6, pp. 065109-06112, Jun 2012

[30] H. Schachter, L. Bergstein, "Noise analysis of an automatic gain control system", *IEEE Transactions on Automatic Control*, vol.9, no.3, pp.249-255, Jul 1964

[31] S. D. Senturia, *Microsystem Design*, Kluwer Academic Publishers, Dordrecht, 2001.

[32] L. E. Frenzel, *Principles of Electronic Communication Systems,* McGraw-Hill, Inc. New York, pp. 93-117, 2008

[33] J. E. Ohlson, "Exact Dynamics of Automatic Gain Control", *Transactions on Communications, IEEE*, vol.22, no.1, pp.72-75, Jan 1974

[34] D. Whitlow, “Design and Operation of Automatic Gain Control Loops for Receivers in Modern Communications Systems”, Analog Devices.

[35] J. P. Alegre Pérez, S. C. Pueyo, B.C. López, *Automatic Gain Control: Techniques and Architectures for RF Receivers*, Springer Science+Business Media, New York, pp. 13-28, 2011.

[36] "Automatic Gain Control AGC", The Great Soviet Encyclopedia, 3rd Edition. 1970-1979. The Gale Group, Inc. 25 Dec. 2014